

Ferroelectrics and multiferroics for next generation photovoltaics

M. A. Jalaja, Soma Dutta *

Materials Science Division, Council of Scientific and Industrial Research, National Aerospace Laboratories, Bangalore 560017, India

*Corresponding author. Tel: (+91) 8025086145; E-mail: som@nal.res.in

Received: 01 March 2015, Revised: 08 April 2015 and Accepted: 28 May 2015

ABSTRACT

Growing energy crisis and environmental issues demand alternative source of green energy. In recent years ferroelectrics and multiferroics have got renewed attention for the breakthrough in photovoltaic application. Multiferroic is an appealing class of material, having two or more ferroic properties intimately coupled to each other. Energy harvesting from ferroelectrics and multiferroics is a pioneering field of research by its own, combination of other ferroic properties is a value addition to it. The coupling of ferroic and optical properties has brought a revolution in the field of photovoltaics. This review highlights recent development in the field of ferroelectric-multiferroic photovoltaics and summarizes the electrical, optical and photovoltaic properties of various ferroelectric and multiferroic systems. The different mechanisms and factors that attribute to the photovoltaic phenomena in ferroelectrics and multiferroics are also described here. Copyright © 2015 VBRI Press.

Keywords: Multiferroics; photovoltaics; photovoltage; photocurrent; bandgap.

Introduction

The field of alternate and renewable energy has experienced a steady and significant growth in the last decade. Among the alternative power sources solar energy is one the most important resources, used widely across the globe. Solar energy harvesting through Photovoltaic (PV) has already been recognized globally. PV solar cell has emerged as the most promising alternative of traditional energy sources depending on the materials, mechanisms and conversion efficiencies [1, 2]. Conventional solar cells are now commercially available in the market which is mostly the first generation silicon based single p-n junction device. Theoretically, the efficiency of the first generation solar cells can reach upto 31% to maximum of 41%, depending on the concentration of solar light [3, 4]. At present, solar cell production is dominated by crystalline silicon modules since they possess relatively high efficiencies and matured fabrication techniques. But the cost of silicon wafers used in solar cell is very high and that is a major issue of power harvesting from photovoltaics compared to existing fossil fuel technologies. Though the second and third generation solar cells are cost effective but their efficiencies are compromised with cost [3, 5].

Second generation solar cells are single-junction or multi-junction devices, mainly focus on thin film based designs [6], developed out of amorphous Silicon [7], Copper Indium Gallium Selenide (CIGS) [8, 9], Cadmium Telluride (CdTe) [10, 11] and polycrystalline Silicon (p-Si) deposited on low-cost substrates like glass [12]. These thin film devices experience the performance limitations similar to the first generation solar cells but they are comparatively

cheaper. The reduction in material usage, use of low cost substrates and large throughput manufacturing are the key points behind the cost effectiveness of second generation solar cells [13, 14]. Multi-junction solar cells are constituted with multiple semiconducting layers in which each junction or sub cell bears unique bandgap to absorb photons from a specific region of the solar spectrum and to convert them into electricity. Use of multi-junctions in these solar cells improve the cell performance to overcome Shockley-Queisser limit (the maximum theoretical efficiency of a solar cell using a p-n junction), but it also increases the complexity and thereby production cost. As per efficiency chart, published by Energy Laboratory (NREL), Fraunhofer Institute for Solar Energy Systems, the highest efficiency reported for second generation solar cells with multi-junctions is 45.7%. The theoretically predicted efficiency value with infinite-junction is 87%. The efficiency of a novel multi-junction solar cell consisting of gallium indium phosphide (GaInP) junction, gallium arsenide (GaAs) junction, and two gallium indium arsenide (GaInAs) junctions is reported about 45.7% which is achieved through lattice-mismatching of each layer to the substrate and even distribution of defects in the active layers [15].

Later, the idea of third generation PV cell evolved, aiming towards combining the merits of both first and second generation solar cells i.e, high conversion efficiency of first generation solar cell and low cost of second generation solar cell. Basically, the third generation solar cells are categorized as dye sensitized solar cells (DSSC) [16-18], organic/polymeric/plastic solar cells [19-21], nanocrystal based solar cells [22, 23], quantum dot solar

cells [24], perovskite solar cells [25] etc. DSSC uses semiconductor based structures formed between a photo-sensitized anode and an electrolyte where, the semiconducting nanocrystals work as antennae to absorb the sunlight and the dye molecule takes the role to separate the charge carriers. Low cost and easy manufacturing are the main attractions of this type of solar cells. But the degradation of cell performance over time and the risk of using liquid electrolyte are the main issues with DSSC. The development of more efficient electrolytes and new broadband dyes which can absorb wide solar spectrum may allow DSSC to compete with the first generation solar cell. Organic solar cells are developed from polymeric or plastic materials. Though, they are not very efficient but potentially a cost effective product. The high-speed and low temperature manufacturing processes and use of standard printing technologies reduce the production cost of organic solar cells. Another attraction of organic solar cell is solution-based fabrication method by using nontoxic materials which are abundant. Light weight, flexibility, transparency and optical tuning are the added feature of organic solar cells which make them potential for mobile applications [25, 26]. Quantum dot solar cells can theoretically overcome the Shockley-Queisser efficiency limit (33.7%) as they can generate more than one electron-hole pair for each absorbed photon. But, the efficiency of Quantum dot solar cell is about 8.6% which is quite low compared to the theoretical value [27]. Use of novel materials, concepts and integration of nanotechnology (quantum dots/wires, quantum wells, or super lattice technologies) may help in achieving the theoretical value. Overall, it is realized that new technologies, advanced materials and architectures needs to be put together in third generation solar cell industry to compete the present market of first generation solar cells.

Very recently, ferroelectric and multiferroic photovoltaics have revitalized third generation solar cells through the discovery of very large photo responses in a few ferroelectric and multiferroic compounds like $\text{Pb}(\text{Zr},\text{Ti})\text{O}_3$ (PZT), BiFeO_3 (BFO) and $\text{Bi}_2\text{FeCrO}_6$ (BFCO). PV effect in ferroelectric (FE) has been discovered about five decades back, though it was least attended till the discovery of large photovoltage (15 V) in BFO thin films [28, 29]. PV effect in ferroelectrics arises from the inherent electric field due to non centrosymmetry, which maintains the charge separation through spontaneous polarization. The developed photovoltage is proportional to the magnitude of electric polarization and separation between electrodes i.e, the thickness of the material [30]. Ideally, it is possible to generate very large photovoltage in ferroelectrics though the photocurrent is low. The recent reports say, low photocurrent is no more a limit for this dielectric class as the new ideas like 'above bandgap large photovoltages' [28], 'role of domain walls' [31], 'effect of thin films' [32] 'tip enhanced PV effects' [33] etc., are developed [34].

Harvesting solar energy from multiferroics is still a new field of research which has got considerable attention in the recent years. The charge and spin of electrons together play a role in multiferroics as it combines two or more ferroic orders like ferroelectric (P), ferromagnetic (M), and ferroelastic (ϵ), which can be switched by their conjugate

electric (E), magnetic (H), and stress (σ) fields respectively. The interesting feature of multiferroic is magnetoelectric coupling where magnetic field can control the electric polarization and vice versa [35-38]. Multiferroics is well known for their application in memory devices, sensors and spintronics [39-43]. Improvements in photovoltaic efficiency have been reported for low bandgap multiferroics [44]. But cross coupling of multiple functionalities (i.e., electrical, magnetic and optical) in multiferroics is a big challenge to understand and design a new material with improved functionalities [45-47]. This report reviews the key factors that contribute to the photovoltaic property in ferroelectric and multiferroic materials and describes various theories that support the photovoltaic phenomena in them. The review highlights recent developments in the field of ferroelectric and multiferroic photovoltaic with a summary of preparation and properties of few standard ferroelectric and multiferroic systems.

Origin of photovoltaic phenomena in P-N junction semiconductors, ferroelectrics and multiferroic materials

P-N junction semiconductors

The solar cell technology is dominated by semiconducting materials. The band gap of these semiconducting materials lies in the visible region of the solar spectrum. The fundamental mechanism behind the PV effect in conventional semiconducting materials is due to the presence of p-n junction. When p type and n type materials are brought together, holes and electrons close to the p-n junction diffuse across the junction towards opposite polarity that creates a space charge region (region of no mobile charge carriers) around the junction, which is also called as depletion region. The electric field existing in the space-charge region of the p-n junction is the source for the separation of the photogenerated charge carriers **Fig. 1**. The semiconducting solar cells when illuminated with light of energy greater than its bandgap energy, light gets absorbed and charge carriers are generated at the p-n junction which are separated by built in voltage at the depletion region by giving rise to a photogenerated current. Theoretically, the quasi-fermi energy difference of electrons and holes formed by light illumination determines the photovoltage in p-n junction solar cells. So the developed photovoltage mainly depends on the bandgap of the semiconducting absorber material [28, 29, 48, 49]. In **Fig. 1** the band bending shows the sharp shift in energy levels of valence and conduction band of p and n type materials.

Ferroelectrics

The photovoltaic phenomenon in ferroelectric (FE) materials is quite different than that of the conventional semiconducting photovoltaics as explained in previous section. In ferroelectrics, single material is responsible for electron and hole pair generation instead of creating a p-n junction of two materials. When solar photon is absorbed by a FE material, the electron hole pair in the dipoles gets separated. Non centro-symmetry that is, breaking of strong inversion symmetry in ferroelectrics sets up an internal field

to effectively maintain the separation between photo excited charge carriers. This can generate huge open circuit voltage (V_{oc}) in ferroelectrics, which may be in the order of above bandgap voltage. But, the efficiency of light-to-electricity conversion in the bulk ferroelectric material is no way close to the conventional p-n junction of solar cells. Moreover, most of the FE materials studied so far for PV application have wide bandgap which restrain them from visible light absorption.

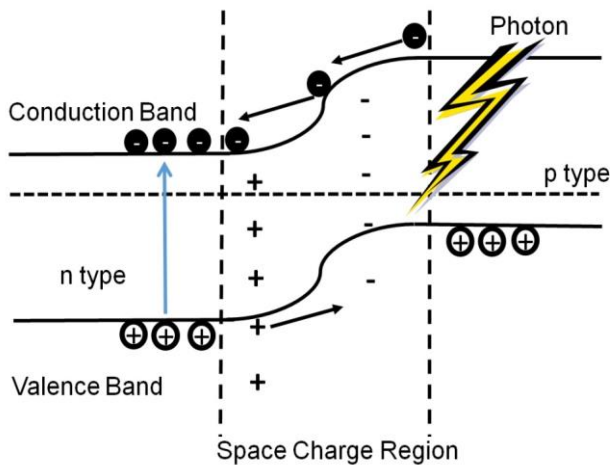


Fig. 1. Origin of photo induced electric field in p-n junction semiconductors.

Since the direction of polarization is switchable in ferroelectric materials by changing the poling direction with the application of suitable electric fields, the direction of photocurrent can also be changed in ferroelectric photovoltaic (FE-PV). A schematic of the FE-PV device structure and origin of electric field in FE materials is shown in **Fig. 2(a)** and **Fig. 2(b)** respectively. Non-centrosymmetry of the unit cell causes asymmetries in electron-light interaction like excitation, relaxation, and scattering processes.

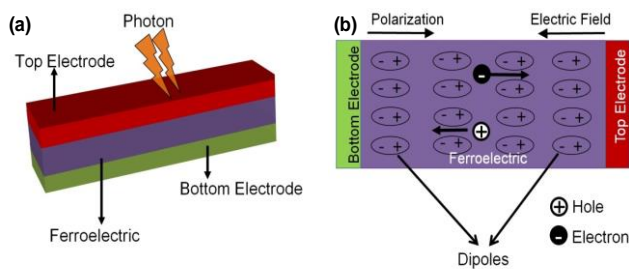


Fig. 2. Schematic of (a) ferroelectric/multiferroic PV device and (b) electric field develops within FE materials.

The photovoltage in ferroelectrics depends on remnant polarization, domain walls, interface between FE-electrodes and Schottky or screening effect as arises from interface beyond the common factors like intensity of incident light, absorption coefficient and bandgap of the material. Photovoltage generation in noncentrosymmetric material is limited, because of wide bandgap value (approximately 3 eV in most of the ferroelectrics) which restricts the absorption of visible light.

In general, the functionality of a PV device is evaluated by measuring its photovoltage and photocurrent. The origin

of large photovoltage in FE-PV is controversial and there are different models to explain its origin on the basis of Bulk photovoltaic effect, Domain wall theory, Schottky-junction effect and Depolarization field model [2].

Bulk photovoltaic effect

PV effect in un-doped, single crystal samples of materials like LiNbO_3 , BaTiO_3 or PZT are reported to be originated as bulk photovoltaic effect, occasionally referred as the photogalvanic effect or non-linear photonics. The noncentrosymmetric nature of these types of materials results in the formation of a steady state current [50].

When light falls on these materials the electron takes off in one particular direction without crossing from one material to another, unlikely, as it happens in common p-n junction semiconductors. There are different models to explain bulk photovoltaic effect which are asymmetric carrier, asymmetric potential well, shift current and nonlinear dielectric models. The simplest model 'asymmetric carrier' is based on the asymmetric carrier scattering centers as explained schematically in **Fig. 3(a)** in which a random diffusion and drift of carriers occurs in the medium, resulting a net flow of photo current [51].

Asymmetric potential well model considers asymmetry in the electrostatic potential at the light absorbing centers which is developed from the dielectric polarization. The asymmetric potential well at the absorbing centre and the movement of electron is shown in **Fig. 3(b)** that explains in the presence of light, carriers are excited from ground state energy level E_0 to E_1 and then E_2 where the potential energies are lesser than ϕ_1 and ϕ_2 respectively. If the excitation energy E_1 is less than the potential ϕ_1 at the absorbing centre, the excited electrons get trapped in the potential well. When the excitation energy is sufficiently large in the order of ϕ_2 or higher, then the carriers diverge from the absorbing centre isotropically causing a lowering in the net current. Only when the energy of excitation E is in between ϕ_1 and ϕ_2 such as $\phi_1 < E < \phi_2$ then there is a net current flow towards the free end of the well. In **Fig. 3(b)** the current flow direction is towards the right. Of course, there is a probability of tunneling of the carriers through the potential barrier ϕ_2 [52].

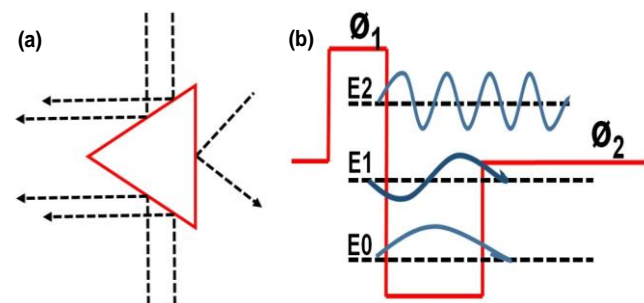


Fig. 3. Different models explaining bulk photovoltaic effect (a) asymmetric carrier scattering centers and random scattering of charge carriers (b) asymmetric potential well at a carrier generation centre.

Shift current model has got much attention in predicting the large photovoltage in bulk photovoltaic accurately [53-55]. In shift current model the FE material is considered as a current source since the conductivity of most FE materials

is very low. In this model, the noncentrosymmetry in the FE crystal gives rise to asymmetry in the momentum distribution of light generated charge carriers resulting in a steady state current. The nonlinear optical processes resulting from the second order interaction with monochromatic light gives rise to a shift current. The electrons are excited to coherent superpositions, which allow the net current to flow from the asymmetry of the potential. The optically induced coherent polarization plays a crucial role in linear and nonlinear light matter interaction. Shift current is a result of real-space shift of carriers during interband excitation. Since the electrons undergo a "shift" in position for each time they absorb a photon this photocurrent is named as a "shift current". **Fig. 4** shows how an electron from an unit cell shift towards right side from A to B by absorbing a photon each time (marked by red arrows) or from B to C by releasing many phonons (marked by black arrows) which is a common phenomenon for electron- electron or electron-photon or electron- phonon interaction.

Though preliminary models assumed that the steady current (J_s) in FE-PV depends on polarization, space charge, defects and impurities [56-57]. But first principle calculation proved that the photocurrent is independent of the magnitude of material polarization but depends on the electronic structure of the material [58]. Of course, the inversion symmetry of the material must be broken, that is common for all theories.

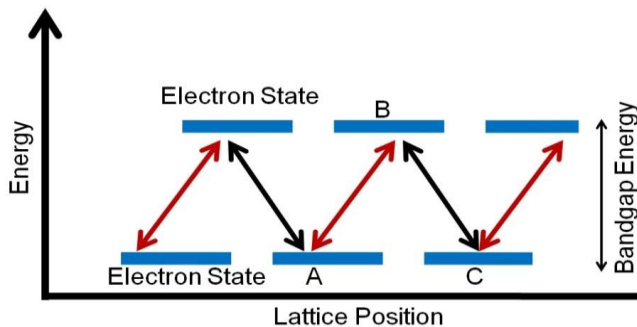


Fig. 4. Electron shift in real space.

Another bulk PV effect is predicted by nonlinear dielectric model where the photocurrent density establishes a correlation between dielectric and optical nonlinearity in FE-PV [59]. When a FE material is illuminated with light then photo carriers and electric field gets generated. The polarization (P) of linear dielectric is directly proportional to the electric field but if the nonlinear effect is considered for dielectric polarization then the expression for polarization can be written as

$$P = \epsilon_0 (\chi_1 E_{op} + \chi_2 E_{op}^2)$$

Where ϵ_0 the permittivity of free space, χ_1 is the linear susceptibility, χ_2 is the nonlinear susceptibility of the second order and E_{op} is the electric field at an optical frequency. The illuminating light is an electromagnetic wave which provides an electric field for charge carriers in

ferroelectrics. When an alternating electric field with amplitude E_{op} and optical frequency ω_{op} is applied to a FE material then the time dependant polarization equation can be written as given below by considering the nonlinear dielectric response;

$$P = \epsilon_0 \{ \chi_1 E_{op} \cos(\omega_{op} t) + \chi_2 E_{op}^2 \cos^2(\omega_{op} t) \}.$$

The above expression contains two parts. For a linear dielectric the second part is zero, the polarization oscillates in optical frequency ω_{op} . In a nonlinear material, light induced polarization contains fundamental polarization wave and higher order asymmetric polarization.

Domain wall theory

Domains represent the spatial extension (about a few microns) of spontaneous polarization vector in FE crystals. Ferroelectric domains are separated from each other by domain wall of 1-2 nm in width [60]. A schematic of domain, domain walls with valence band and conduction band across these domains is shown in **Fig. 5**.

Domain wall theory says, separation of photogenerated charge carriers happens only at the domain walls, due to the variable periodic potential structure of the domain [58]. The probability of recombination of charge carriers is minimum at the domain wall that produces electric field corresponding to each domain resulting a net diffusion current. Photo voltage produced by this process at multiple domain walls (periodically ordered) gets added up in series and generate above band gap photovoltage. As per domain wall model, the photocurrent does not depend on the direction of light but it depends on polarization direction. So the current produced by the bulk PV effect may partially get cancelled or added up depending on the direction of current produced by domain wall. If the photocurrent, generated by, bulk PV phenomenon and domain wall effects are in the same direction, then the power conversion efficiency gets amplified [2, 58]. Domain wall theory is inept of explaining the entire PV phenomenon in ferroelectrics.

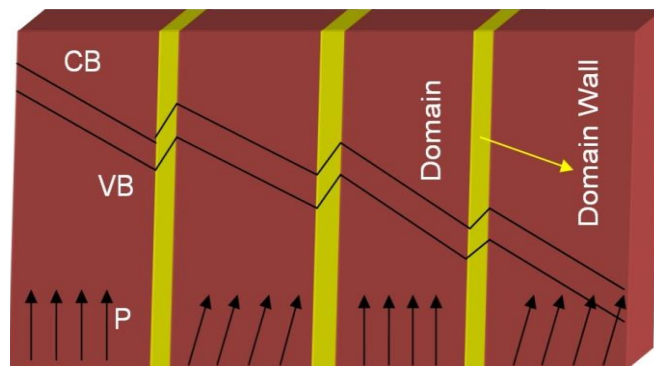


Fig. 5. Schematic of domains and domain walls (DW) with corresponding band diagram of valence band (VB) and conduction band (CB).

Schottky-junction effect

The interface of FE material and metallic electrode forms a Schottky junction where a local electric field is produced.

Due to the local field the charge separation happens at the junction when light energy falls on it which leads to a photocurrent. The magnitude of photovoltage is negligible at the Schottky-junction of the bulk ferroelectrics (significant in the case of thin films). In a metal/ferroelectric/metal structure, the local internal electric field (E_1) develops at the Schottky barrier is defined as $E_1 = E_{I-Bottom} - E_{I-top}$ where, $E_{I-Bottom}$ and E_{I-top} are the Schottky barriers between the bottom and top electrode/ferroelectric respectively. The photocurrent in metal/ferroelectric/metal structure depends on the height of the Schottky barriers at the top and bottom interfaces, which in turn relates the percentage of interface charges. It is observed that the bigger the difference of height of Schottky barrier at the bottom and top interfaces, larger the photocurrent [61, 62].

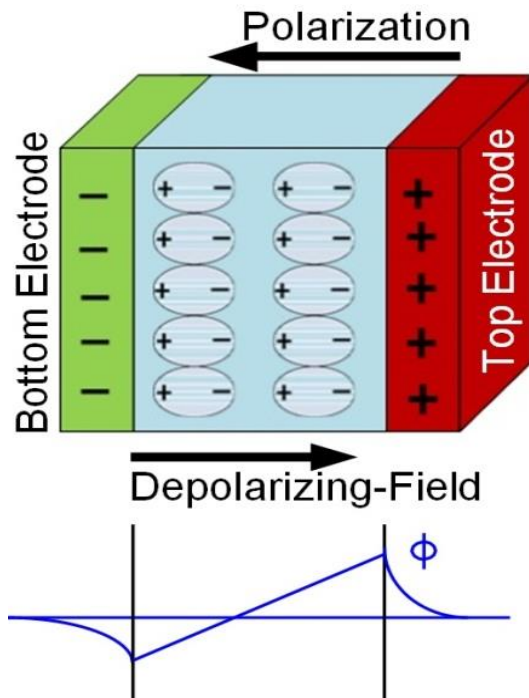


Fig. 6. Screening of polarization charges and distribution of electrostatic potential (ϕ) in a FEPV structure with dissimilar electrodes.

Depolarization field model

Another important theory that based on depolarization field, explains the occurrence of high photovoltage in ferroelectric thin films. The unscreened polarization charges on the surface of the polarized ferroelectric thin films act as a source for the depolarization field Fig. 6.

The screening of surface charges depends on the remnant polarization, dielectric constant, thickness and charge density of the FE material and metal electrode. As the depolarization field is directly proportional to the strength of polarization, it can be tuned by varying the external bias voltage. The screening effect which suppresses the depolarization field is more prominent in metal/ferroelectric/metal electrode structures and negligible in oxide/ferroelectric/oxide electrode structures [63]. The effect of depolarization field contributes more towards photocurrent than photovoltage. But this effect is evident in ferroelectric thin films of thickness in the order of 100nm. Photovoltaic phenomenon in different ferroelectrics,

dominated by the factors discussed above are reviewed and summarized in Fig. 7.

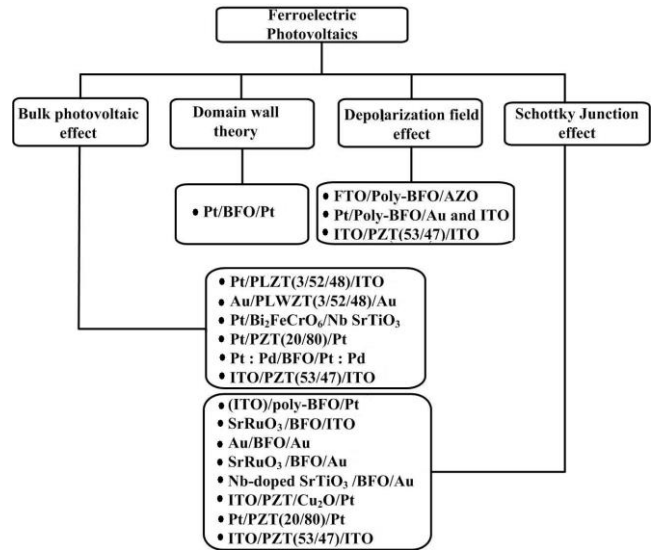


Fig. 7. Different FE-PV devices and dominating factors for the origin of photovoltaic properties in them [28, 32, 33, 63, 64, 75].

Multiferroic

More recently a new origin of photovoltaic phenomena from the spin property of the electron called as spin photovoltaics is also realized [76, 77] for the class of materials called multiferroics. Though the ferroelectric polarization plays the major role in producing PV effect in multiferroics still there is a contribution of magnetic spin also. The advantage of multiferroics over ferroelectrics is their low bandgap energy. The electron-electron interaction governing the magnetic ordering results in low band gap values in them which facilitate the flow of improved photocurrent in multiferroics. Moreover, the ferroic properties in multiferroics enable the tuning of photovoltaic properties with the manipulation of electric and magnetic field. Low band gap energy of multiferroic favors the absorption of light in the visible to near infrared region which constitutes the major part of energy in the solar spectra [44].

Photovoltaic phenomenon due to magnetic spin is under conceptualization and development stage. In a nonrelativistic description, all valence band electrons have an equal probability of being excited by photons. Spin based photovoltaic phenomena arises from the electron transition between spin splitted subbands. When the bands are splitted by spin-orbit coupling, the momentum of the excited carrier depends on its spin. Spin orbit interaction in asymmetric potential results in the splitting of electron energy bands correspond to spin up and spin down state, which gets shifted in k (momentum) space. Therefore, illumination of polarized light results in flow of current. Clockwise polarized light excites electrons to a momentum state $k_z > 0$ and anti-clockwise polarized light excites electrons to $k_z < 0$, because of the decoupling of the spin channels (Fig. 8). The nature of the splitting may be different for electrons and holes due to the different orbital contributions to the conduction and valence bands [78]. Fig. 8 shows the splitting of the conduction band in two

spin states ($\pm \frac{1}{2}$) in the y direction. If one of the spin sub bands is occupied then asymmetric spin flip scattering occurs resulting a small current in the z direction.

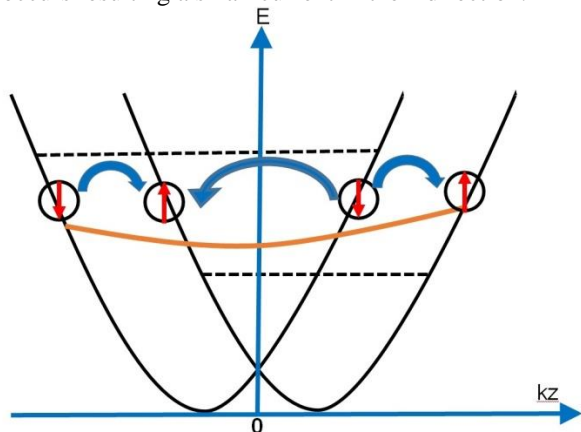


Fig. 8. Spin orbit interaction in asymmetric potential resulting a splitting of electron energy bands to spin up and spin down state in multiferroics.

Recent studies on multiferroic BiFeO_3 has reported high photovoltage which is attributed to particular magnetic domain arrangement [79, 80].

It is hypothesized that the life time of excited states in multiferroic materials are enhanced due to spin dependent transition selection rules where strong spin-orbit interaction gives rise to unusual opto-electronic properties [77, 81].

Ferroelectric Materials for Photovoltaics

Perovskite structured ferroelectrics are most suited for PV application because of their polar non centrosymmetric nature. There are other advantages of using perovskite structured oxides since they are cheap, easy to manufacture in traditional laboratory, abundant in nature and few of them are environment friendly too. In this section few common ferroelectric materials PZT, barium titanate (BT), lithium niobate (LiNbO_3) and modified potassium niobate (KBNO) are reviewed for their applications in photovoltaics [82-84].

PZT

PZT is a well-known material because of their excellent dielectric, ferroelectric, piezoelectric, pyroelectric properties but the literature on photovoltaic properties of PZT is scant. Recently PZT has occupied a significant place in the FE PV world due to improved PV efficiency. An efficiency of 1.25% is reported in PZT thin film when they are grown on n type Si with ingenious oxide engineering [85]. $\text{Pb}(\text{Zr}_{0.53}\text{Ti}_{0.47})\text{O}_3$ sandwiched structures grown on glass substrates with ITO as top and bottom electrodes showed a PV efficiency of 0.22% which is tunable with external electric field [63]. The increase of Zr content in PZT increases the band gap from 3.9 to 4.4 eV which allows the photocurrent to generate in ultra violet (UV) region making them suitable as UV detector. Enhancement in PV efficiency of PZT is possible through energy level engineering by inserting semiconducting materials as buffer layer at the metal/FE/metal interfaces or by incorporating the semiconducting materials like Ag_2O or Cu_2O into the matrix [86]. The inclusion of n type Cu_2O as

a buffer layer in ITO/PZT/ Cu_2O /Pt thin film structure gives large short circuit current density and enhanced PV efficiency (0.57%) closer to the order of inorganic solar cells [78]. Lanthanum modification in PZT changes its photoresponse from UV region to visible region with overall enhancement in PV properties. Since low work function of metal helps in emitting the photo electron, the effect of different metal electrodes (having low work function) has been observed in pure and modified PZTs. With Mg electrode short-circuit current of La modified PZT (PLZT) gets enhanced by 150 times than that of the Pt electrode [86]. Enhancement in PV efficiency is reported for PLZT with nitrogen doping [87].

Pb vacancies in the perovskite structure improve the PV properties in PZT. The process parameters during sintering/annealing also play important role to improve optical properties in PZT. Increase in photovoltage and photocurrent with decrease in oxygen partial pressure during the heat treatment of PZT prepared by solid state reaction method is reported [88]. Heat treatment of the same PZT in nitrogen atmosphere increases photovoltage and photocurrent remarkably at high temperatures (above 1123 K). The PV effect is prominent in PZT when the molar ratio of $\text{Pb}/(\text{Zr}+\text{Ti})$ is less than 1 [89].

The performance of a PV device depends on carrier density, life time of photogenerated charge carriers, and mobility of carriers. Presence of intergrain boundaries, defects, dislocations, misfit, domain wall orientation etc. are the factors which affect the carrier density and mobility. Theoretically predicted photovoltaic efficiency in ferroelectrics is very less ($\sim 10^{-6}$ - 10^{-4}) due to the short life time of photogenerated charge carriers. Most of the ferroelectrics are of p type and hence, the electron concentration is less in them compared to the +ve charge carriers (holes/ions). The larger effective mass ($m^* = 5$ - $6.7 m_e$) of these p type carriers in FE materials reduces the mobility of +ve charge carriers which intern reduces their contribution towards photoresponse. The oxygen vacancies create ionic mobility in FE materials which is around 10 - $12 \text{ cm}^2(\text{Vs})^{-1}$ [90]. The mobility of electrons in FE material is less and typically of the order of 0.1 to $3.0 \text{ cm}^2(\text{Vs})^{-1}$ [90]. La doped PZT (PLZT) shows carrier mobility $100 \text{ cm}^2(\text{Vs})^{-1}$ and carrier life time of 200 ps [90]. Radiative lifetime value calculated in Nd doped PZT is $165 \mu\text{s}$ [91]. N type conductivity of PZT is reported with PZT/Pt thin films, where the electron mobility is twice than that of the mobility of holes [92].

The absorption coefficient of a material determines how far light of a particular wavelength can penetrate into that material before it gets absorbed. PZT has higher absorption coefficient in the UV region. The absorption coefficient values with the variation in Zr content in PZT are graphically represented in Fig. 9(a) [93].

PZT thin films show temperature dependent absorption coefficient this is related to the effect of temperature on the band gap values. Bandgap values in PZT are seen to decrease with temperature as seen in Fig. 9(b). The variation of refractive indices with different photon energies in $\text{Pb}(\text{Zr}_{0.6}\text{Ti}_{0.4})\text{O}_3$ is shown in Fig. 9(c) [93-98].

Photovoltaic properties (efficiency, photo voltage and photocurrent density) of various PZT based PV devices are compared in Fig. 10(a). The maximum efficiency in PZT is

reported to be 1.25% in a bilayer structure of PZT with n type Si. PZT samples with ITO as top layer shows much improvements in photovoltaic efficiency comparing to other top electrodes. PZT based device can generate large photo voltage with ITO top electrode and large photocurrent density with an intermediate Cu_2O layer in between PZT and bottom Pt electrode as shown in **Fig. 10(b)**.

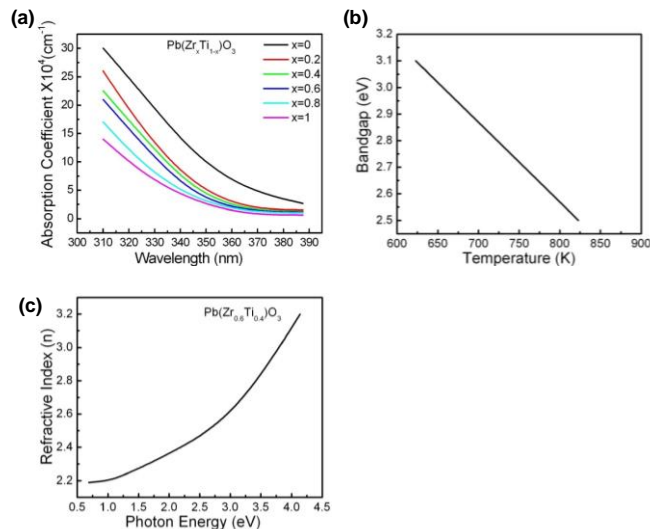


Fig. 9. (a) Variation of absorption coefficient in PZT with different values of Zr content (b) Dependence of bandgap on temperature and (c) Variation of refractive indices with photon energies in $\text{Pb}(\text{Zr}_{0.6}\text{Ti}_{0.4})\text{O}_3$.

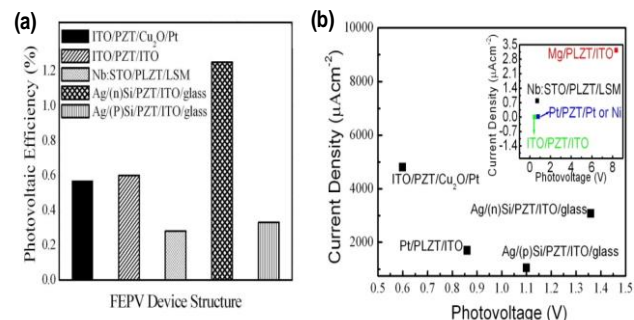


Fig. 10. (a) PV efficiency (b) Photovoltage and photocurrent density of various PZT based PV devices [2, 85].

Lead Free FE- PV

Among the lead free category of FE materials BaTiO_3 , LiNbO_3 and modified KNbO_3 are at the fore front. In the following section the interesting photovoltaic properties of these materials are discussed briefly.

BaTiO_3

Barium titanate is a classic ferroelectric material with perovskite structure. It has spontaneous polarization of 261 Ccm^{-2} and curie temperature of 408 K. It shows other structural transitions at 278 and 180 K. Photovoltaic effect in BaTiO_3 (BT) was first reported in 1956. Like other ferroelectric materials, BT has wide bandgap ($\sim 3.2 \text{ eV}$). More recently this material has received a great attention due to the occurrence of anomalous photo voltage (\sim several kV) in it [99]. Bulk PV effect in BT arises from the non-uniform distribution of spontaneous polarization.

Above Curie temperature BT single crystal shows a weak photovoltaic effect. BT gives a non-steady state photovoltaic current when illuminated by 300 W xenon lamp. Under illumination, photogenerated electrons are trapped at the grain boundaries giving rise to a space charge field. This space charge field results in domain switching and increase the remanent polarization to produce a non-steady state photovoltaic current. The maximum photocurrent (4 nA) was reported with a polling field of 1.5 kVmm^{-1} in the BT ceramic [100].

Bulk absorption coefficient of BT is $5 \times 10^{-2} \text{ cm}^{-1}$ [101]. The variation of absorption coefficient in BT thin film with different photon energy is shown in **Fig. 11**. The experimentally obtained values for absorption coefficient are less compared to theoretically calculated values [102].

An open circuit saturation voltage corresponding to the field of 24 kVcm^{-1} is observed in BT thin films prepared through RF sputtering. Photo voltage is switchable with polarization direction. With the increase in poling voltage, photovoltage is found to increase till saturation of remanent polarization [103]. The photovoltaic efficiency is higher (1%) in BT thin film compared to the bulk BT crystal. At the light intensity of 400 mWcm^{-2} a photovoltage of 7.6 was reported in BT [101].

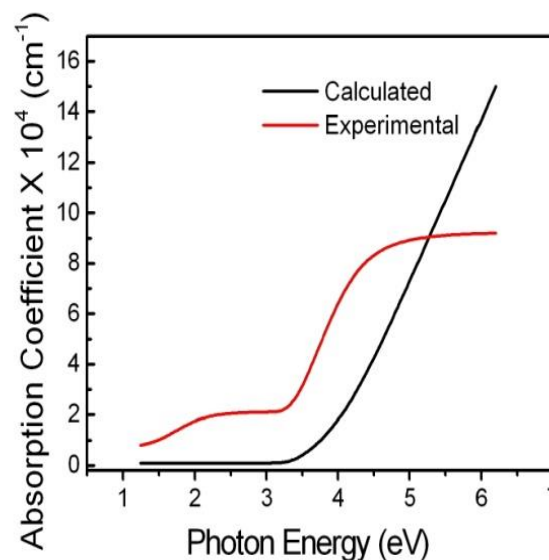


Fig. 11. Variation in absorption coefficient in BT thin film.

LiNbO_3

LiNbO_3 is the first human made dielectric material with very high Curie temperature (1483 K) and large spontaneous polarization (0.70 Cm^{-2}). PV effect in LiNbO_3 crystals was observed in 1969 [104]. The PV phenomena in LiNbO_3 arise mainly from bulk photovoltaic effect. In early days it used to be considered that LiNbO_3 is suitable for ultraviolet photo detectors due to its large bandgap value ($\sim 4 \text{ eV}$). Later it was found that these crystals can respond to all wavelengths e.g; ultraviolet, visible, and infrared radiation of light. The generated photovoltages in LiNbO_3 increase linearly with the energy of light. The variation of photovoltage in LiNbO_3 with laser light energy is shown in **Fig. 12**. LiNbO_3 has a typical ultrafast photoresponse time of 2 ns and further reduction of photoresponse time is possible if the crystal is made thinner.

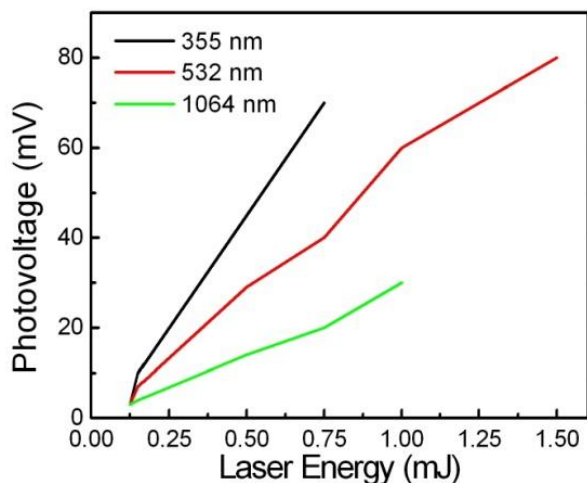


Fig. 12. Photovoltage in LiNbO₃ crystal at different wavelengths.

Defects in LiNbO₃ crystals improve the PV performance of this material [104]. The main intrinsic defect in this material originates from the bipolarons and small polarons. When electron transition happens between these defect levels and conduction band, photocurrent produces. LiNbO₃ possess two optical absorption peaks as shown in Fig. 13. The bigger one (photon energy 4 eV) corresponds to ‘band to band absorption’ and the smaller one (photon energy 1.97 eV) correspond to absorption between ‘bipolarons and small polarons’.

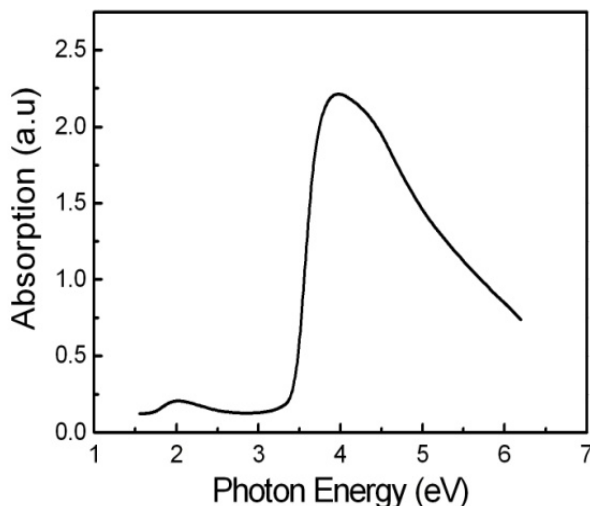


Fig. 13. Absorption spectra for LiNbO₃ crystal.



KBNNO is a recently developed perovskite oxide. It exhibits both ferroelectricity and visible light absorption with direct bandgap in the range 1.1-3.8 eV [105]. KBNNO belongs to the parent material KNbO₃, a class of FE perovskites with ABO₃ structure. Potassium niobate (KNbO₃) is a promising lead free FE material with wider bandgap of 3 eV. Barium nickel niobate (BNNO) is a good absorber of visible light due to its low bandgap which is attributed to the ionic bonding between the constituent elements and oxygen. The substitution of BNNO in KNbO₃ brings out attractive FE properties in the resultant KBNNO

with a low bandgap (1.39 eV). A plot depicting the bandgap values of KBNNO with different BNNO percentage is shown in Fig. 14. By tuning the composition of KBNNO, bandgap values can be widely varied in this material. Visible light absorption is also possible by adjusting its bandgap near to 1.5 eV. The best-measured electric polarization reported in the FE KBNNO is ~0.2 Cm⁻². The absorption coefficient value in KBNNO is approximately 1.2×10⁴ cm⁻¹ corresponding to the bandgap value of 2 eV (Fig. 15).

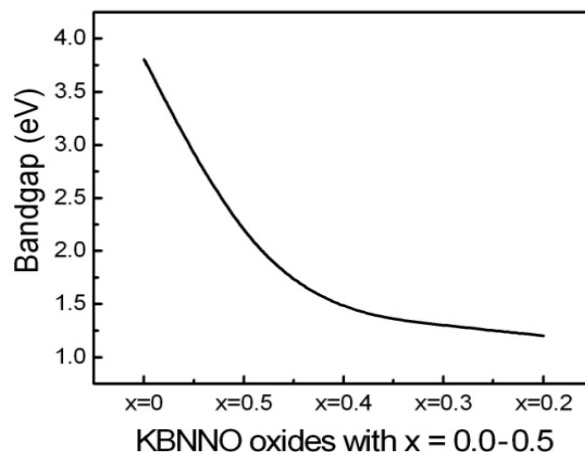


Fig. 14. Variation of bandgap in KBNNO at different BNNO (x) values.

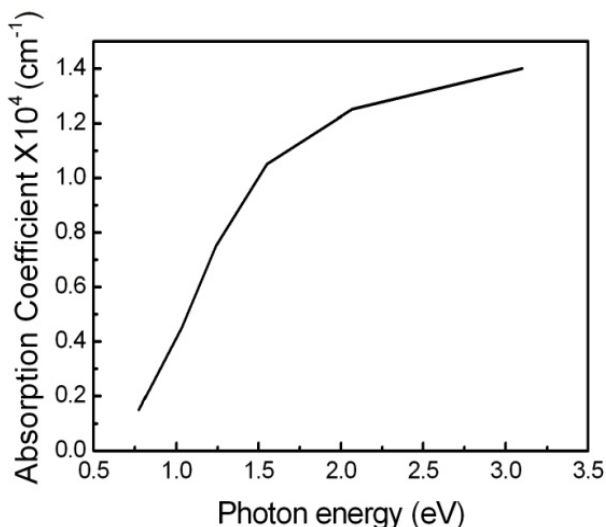


Fig. 15. Absorption coefficient in KBNNO.

Bulk KBNNO gives photovoltage of 0.7 mV and photocurrent of 0.1 μAcm⁻² after poling when illuminated with a light of intensity 4 mWcm⁻². A reversal in photo current with change in poling direction is reported. An efficiency greater than 3% is expected for thin film of this compound. The photoresponse of KBNNO in the visible region of solar spectrum is given in Fig. 16.

An optimal KBNNO composition for solar cell application as evolved theoretically is [KNbO₃]_{1-x}[BaNi_{1/2}Nb_{1/2}O_{3-δ}]_x with different ratios of KNbO₃ and BNNO (x=0.1-0.5) which is validated experimentation by preparing the solid solutions of the same. Enormous potential and opportunities lies in this material which can possibly bring out state of the art optoelectronic devices.

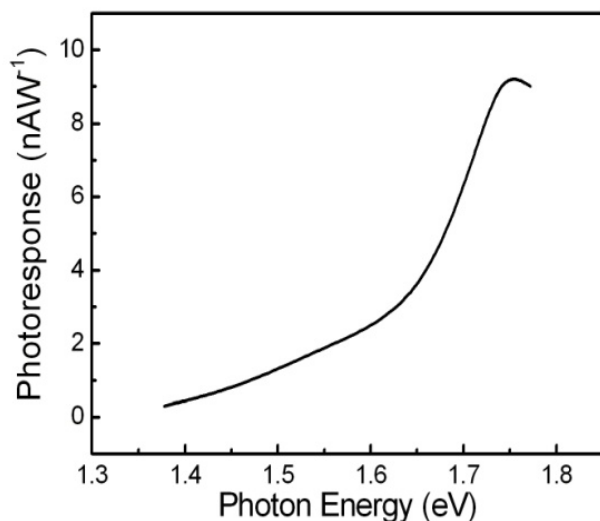


Fig. 16. Photo response in KBNNO.

Multiferroic Materials for Photovoltaics

Multiferroic oxide materials have created a boom in the field of photovoltaics due to the coexistence of ferroelectricity and magnetic order with low bandgap. New materials are developed, different structures and compositions are also designed to enhance PV performance of multiferroics. Out of large number of multiferroic materials studied so far for PV applications, BFO is the most potential candidate. Some of the multiferroic materials and their PV properties are discussed in this section.

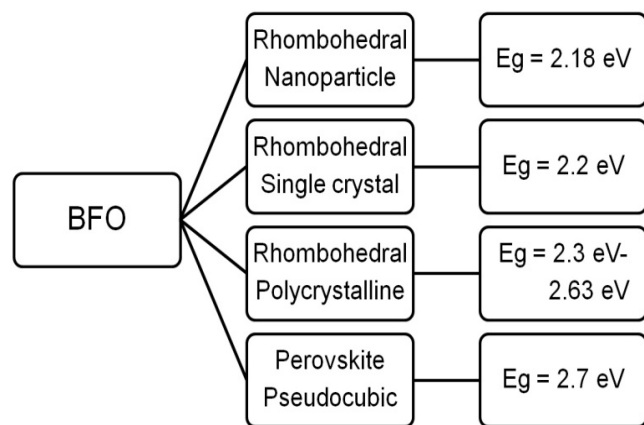


Fig. 17. Band gap values of BFO material with different crystal structures.

BFO

BFO is a promising material, studied well for its ferroelectric, magnetic and PV properties [32, 106-111]. The low band gap energy and high remnant polarization (50-150 μCcm^{-2}) [32, 112] are the important parameters which controls the PV properties of this material [109-111]. The optical bandgap of BFO lies in the range 2.3 to 2.8 eV at room temperature (Fig. 17) which is almost double than that of the values suitable for solar cell application (1.4 eV) [113].

This limitation can be resolved by narrowing the bandgap by strain engineering. By applying uniaxial/hydrostatic pressures externally or by lattice mismatching or chemical pressure strain can be developed in the lattice structure of BFO. Uniaxial compression to R3 rhombohedral structure of BFO can reduce the bandgap which has been predicted by first principle study based on Density Functional Theory [57]. Compressive stress can result in a transformation from indirect band gap to direct bandgap in this material, so that optical absorption improves in higher magnitude [57, 58].

The Anomalous Photovoltaic (APV) behavior (where the photovoltage is a few orders larger than bandgap of the FE material) in BFO thin films have attracted scientific community to investigate next generation photovoltaics [114]. The effect of domain walls in the PV properties of BFO thin films have been studied widely [28, 33]. The origin of huge photovoltage in BFO thin film is 71° and /or 109° nano domain walls. The photovoltage increases linearly with the total number of domain walls along the net polarization direction (direction perpendicular to the domain walls) [28].

In the case of BFO single crystals, the photo generation of charge carriers and their recombination are mainly affected by shallow energy levels, since domain walls have no significant role to play in bulk photovoltaic effect. The photo excited carriers are uniformly distributed over the entire crystal and they do not recombine greatly within the domains. Thus, within the domain, the life time for generation and recombination of photo excited charge carriers is large compared to the domain walls [28, 73]. Carrier life time value reported for BFO bulk and thin film is 15 ns [115]. But there is a drastic increase (190 μs) in carrier life time in BFO nanowires due to the presence of built-in potential which significantly increases carrier recombination life time. The high value of carrier life time in nanowires comes from the defect induced space charge. Nanostructures have large surface to volume ratio and excess surface states that induce trapping of charge carriers when releases with the illumination of light. In general, the depolarization field in the ferroelectric separates out the photogenerated charge carriers in opposite direction before. The oxygen vacancies in BFO dominate n type semiconducting behavior in it. The room temperature resistivity of BFO nano wires is $\sim 3.8 \Omega\text{cm}$. The mobility value calculated in this material is $3 \text{ cm}^2(\text{Vs})^{-1}$ which gives a carrier concentration at room temperature as $5.4 \times 10^{17} \text{ cm}^{-3}$ [116].

In contrast to the FE applications, PV applications require a large leakage current and a large coercive field (E_c) for improved and stable solar cell performance. Many studies were carried out on the effect of various dopants on the FE and PV properties of BFO perovskite (ABO_3) structure. A site Nd doping in BFO has shown an increase in leakage current and coercive field followed to an enhanced PV response [117]. By introducing defect levels in optical band, electron transport and photocurrent can be enhanced in BFO. Same has been tried for BFO nanotubes with Pr and Cr doping and resulted in substantial increase of power conversion efficiency. The incorporated defect levels through metal doping improve the electron mobility [118]. Oxygen vacancies can also improve the PV response

in BFO which is generally created by doping BFO with Ca at the Bi site [119]. Occurrence of structural change (rhombohedral to orthorhombic phase) by Gd doping in BFO enhances the electron concentration and electrical conductivity which contribute largely in photocurrent generation [120].

Effect of electrode on PV properties is theoretically predicted and experimentally proven in the case of BFO. Oxide top electrode on FE capacitor provides a very large depolarization field [72]. Replacement of Au electrode with ITO on Au/BFO/Pt/Ti/SiO₂/Si structure gives large PV response (25 times more). ITO has high transmittance (80%) in the visible region and provides a high depolarization field to separate the photo generated electron-hole pair. Al doped ZnO is a potential substitute for ITO with a merit of high transmittance (~80%), low resistivity ($2-4 \times 10^{-4} \Omega\text{cm}$), low cost and non toxicity [72]. The effects of dopants and electrodes on the PV responses of BFO are summarized in **Table 1**.

Table 1. Effect of dopants and electrodes on PV responses of BFO.

Device Structure	Open circuit photovoltage (V)	Short circuit photocurrent (mAcm ⁻²)	Light intensity (mWcm ⁻²)	Efficiency (%)
Pt/BFO/Pt	16	0.12	285	–
ITO/BFO/SRO	0.8-0.9	1.5	285	10 (EQE) [*]
ITO/15%Ca-BFO ceramic/Au	0.46	2×10^{-5}	91	–
AZO/BFO/FTO	0.63	0.13	100	7 (EQE)
Au/BFO/FTO	0.4	0.043	100	–
Ag/Pr Doped BFO NT/Ag	0.21	8.9×10^{-7}	100	0.5
CRO [*] coated LAO [*] /BFO-BCO [*] /ITO	1.2	0.013	100	0.01
Au/BCFMO [*] /ITO	0.325	0.241	95	0.02
ITO/poly-BFO/Pt	0.1	2×10^{-7}	450	–
graphene/BFO/Pt	2.8	2.8	100	–
Au/BFO/Au	0.08	8.219×10^{-3}	20	–
SRO/BFO/Au	0.286	4×10^{-4}	750	–
Pt: Pd/BFO/Pt: Pd	6 to 30	10^4-10^5	40000	40 (IQE) [*]
Nb-doped STO/BFO/Au	0.15	6	285	0.03

^{*}External quantum efficiency- (EQE), Internal quantum efficiency- (IQE), DyScO₃-DSO, SrRuO₃-SRO, Al doped ZnO- AZO, NT- Nano tube, CaRuO₃- CRO, LaAlO₃-LAO, BiCrO₃-BCO, Ce-Mn co doped BiFeO₃ - (BCFMO), [Bi_{0.9}La_{0.1}][Fe_{0.97}Ta_{0.03}]O₃ (BLFTO) [2, 28, 32, 72, 73, 118, 121-125].

Improved efficiencies are also reported in dye sensitized BFO based solar cells (DSSC). A recent report has shown a power conversion efficiency of 3.85% in the Gd doped BFO based DSSC. Visible light induced size changes in BFO crystals has opened up a new window for next generation wireless devices including light-controlled elastic micro motors and micro switches. The combination of PV and piezo electric effects in the BFO crystals is a prosperous research avenue in the field of photostriction-the light induced deformation [126].

The optical parameters in BFO are highly dependent on processing temperature. An increase in absorption coefficient with increase in processing temperature is seen in BFO material (**Fig. 18**). The bandgap value in BFO is found to decrease from 2.75 eV to 2.7 eV when the processing temperature is increased from 450 K to 650 K (**Fig. 19**).

BFCO

BFCO a new member of oxide multiferroics, has shown potential signature on photovoltaics. It is a type I

multiferroic where ferroelectricity arises from $6s^2$ lone pair of Bi³⁺ ions and magnetism arises from ferrimagnetic behavior. A ferro/antiferromagnetic coupling within Fe-O-Cr bond gives strong magnetism depending on the strength and angle of the superexchange interaction between the Cr³⁺ and Fe³⁺ cations. It is predicted from abinitio calculations that BFCO is having a double perovskite structure with a remnant polarization about $80 \mu\text{Ccm}^{-2}$, and a magnetization of 160 emucm^{-3} at absolute zero [69].

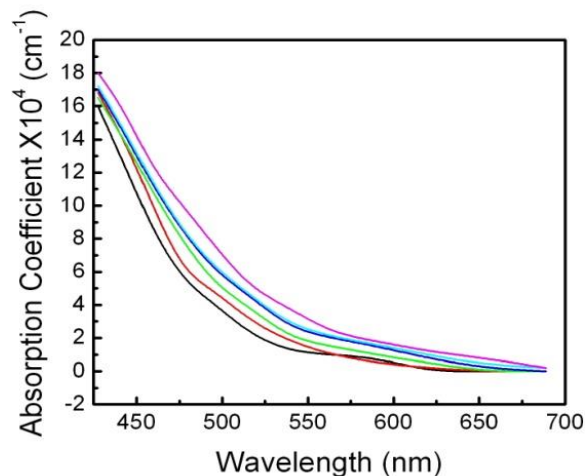


Fig. 18. Variation of absorption coefficient in BFO with increase in processing temperature.

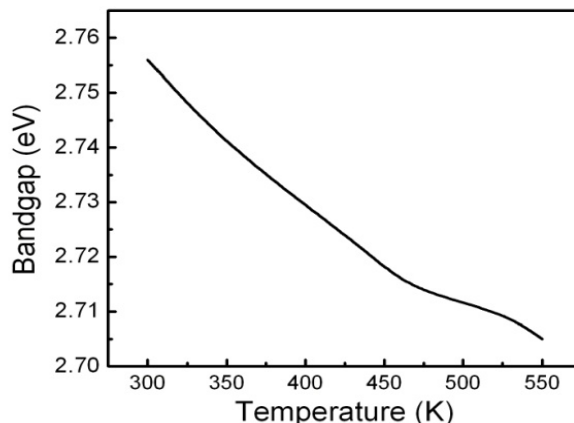


Fig. 19. Temperature dependence of Bandgap in BFO.

Epitaxially grown BFCO thin film gives a polarization of $2.8 \mu\text{Ccm}^{-2}$ and a saturation magnetization of 20.8 emucm^{-3} . BFCO in bulk or in epitaxial thin films is isostructural to BFO with a rhombohedral distortion. It has remnant polarization about $55 \mu\text{Ccm}^{-2}$ along (001) pseudocubic direction at room temperature depending on Fe/Cr ordering. Monte Carlo simulation of the classical Heisenberg model predicted the magnetic curie temperature of BFCO at 450 K by Fe/Cr cation ordering which imbues a strong magnetism in it [69]. The weak ferromagnetism in BFCO originates from the antiferromagnetic coupling between neighbouring Fe (d^5-d^5) and Cr (d^3-d^3) through a slight canting of the spin structure. Fe-Cr ordering in BFCO causes hybridization of d levels in the transition metal atoms Fe and Cr with p bands in oxygen. This large hybridization determines the interatomic distance which decides the optical bandgap in this material. Magnetic

ordering drastically decreases with film thickness above 80 nm, due to the formation of defects [127]. Bulk photovoltaic effect in BFCO at the wave length 635 nm is observed. The conversion efficiency in BFCO with red light illumination reaches 6% in ITO/(001)-oriented BFCO/STO:Nb heterostructure. The high efficiency of the particular BFCO PV cell may be attributed to the high degree of B-site cationic ordering between Fe and Cr sub lattices. Fe-Cr ordering can also be controlled through magnetic field and there by an improvement in the PV efficiency [69, 127-129]. The latest report with a very large power conversion efficiency of 8.1% in BFCO thin-film solar cells is a breakthrough in the field of multiferroic photovoltaics [128]. The spectacular work demonstrated a new approach to effectively tune the bandgap of the double perovskite BFCO oxide by tailoring Fe/Cr cationic ordering. The effect of cationic ordering may be observed with the effect of temperature and deposition time in BFCO thin films. The variation of absorption coefficient with photon energy corresponding to different cationic ordering is shown in Fig. 20(a). The bandgap value of this material is highly dependent of cationic ordering Fig. 20(b). Photovoltaic efficiency of this material can be improved in a multifold by stacking multiple layers of this compound in a sequential manner or by ordered grain growth. These multi layers could absorb light in the range 1.4- 3.2 eV of the solar spectrum [109]. BFCO coating on traditional single-crystal silicon solar cell can improve the solar cell efficiency from 18 to 24% [126].

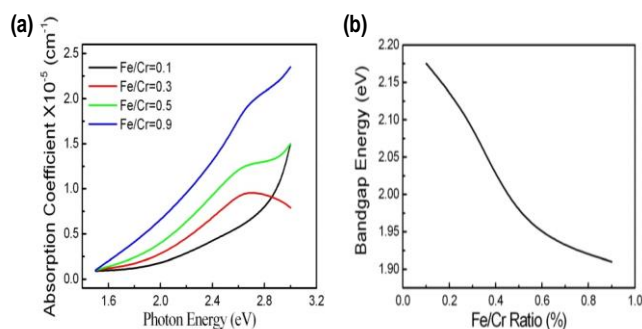


Fig. 20. (a) Variation of absorption coefficient in BFCO with different Fe/Cr ratio and (b) Change in bandgap values with variation of Fe/Cr ratio.

KBiFe₂O₅

The hypothetical concept of lowering band gap in tetrahedrally coordinated compounds has come into reality by the discovery of a new multiferroic KBiFe_2O_5 . This interesting multiferroic compound belongs to a tetrahedrally coordinated $\text{A}_2\text{B}_2\text{O}_5$ structural family with weak ferroelectric and ferromagnetic properties. The structure of KBiFe_2O_5 contains tetrahedral Fe^{3+} in a Fe_2O_3 block that alternates with a (K, Bi) O_2 block. KBiFe_2O_5 , is an extraordinarily interesting material from the point of having very low bandgap value of 1.6eV (direct bandgap), enabling high visible light absorption and higher concentration of carriers for energy transportation. The robust photoelectric effects in the polar, orthorhombic KBiFe_2O_5 has become a revival in multiferroic PV research because of the high photovoltage ($V_{oc}=8.8 \text{ V}$) and photocurrent density ($J_{sc}=15 \mu\text{Acm}^{-2}$). Like other oxide

multiferroics, KBiFe_2O_5 also possess a weak ferromagnetism from the canting of G type antiferromagnetic ordering with a Neel temperature of $\sim 560 \text{ K}$. It shows the FE properties below 780 K and above which it transforms to an antiferroelectric phase. Finally, above 850 K, the material becomes paraelectric. The resistivity of the material is three orders less than that corresponds to the well known BFO. The value of absorption coefficient is $>10^4 \text{ cm}^{-1}$, which is the optimal value for solar cell application. The variation of absorption coefficient in this material with different photon energy is shown in Fig. 21. Together, these results leave no doubt that there is strong photoelectric effect in polar, orthorhombic KBiFe_2O_5 [44].

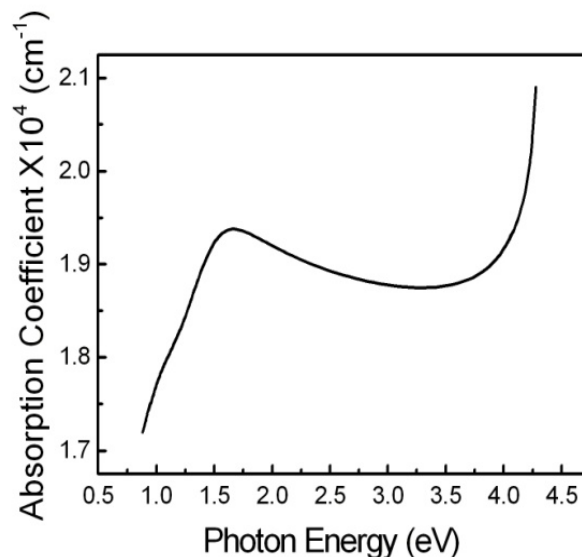


Fig. 21. Variation of absorption coefficient in KBiFe_2O_5 .

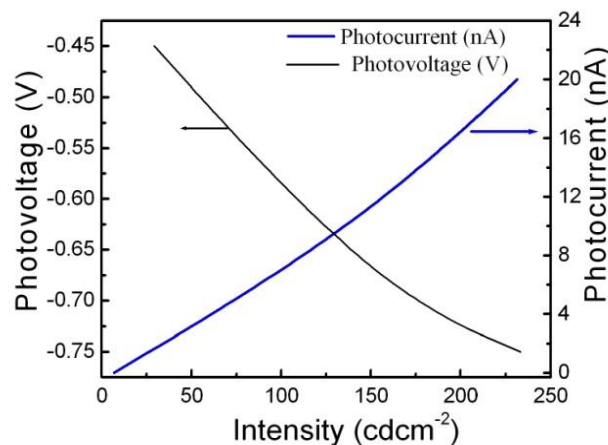


Fig. 22. PV response in PFV at different illumination intensities.

Pb(Fe_{1/2}V_{1/2})O₃ (PFV)

PFV is an excellent candidate for visible light photovoltaics due to its lower bandgap energy and comparatively higher photo voltage and photocurrent. It has got more attention among the group of emerging multiferroics discovered recently. PFV comes under the group of materials having general formula $\text{Pb}(B', B'')\text{O}_3$ ($B' = \text{Mg, Fe}$ & $B'' = \text{Nb, Ta, V}$ and others) and possess perovskite structure. The lower bandgap energy and oxygen vacancies in its perovskite

structure facilitate n-type semiconducting property in this material. The concern is the high leakage characteristics. Moreover, due to the leakage current, remanent polarization reduces which is a primary requisite for light induced electron-hole pair generation to realize PV effect. Separation of light induced charge carriers may be accelerated in this material by inducing defect or concentration gradient through the migration of positively charged oxygen vacancies under application of an external electric field. Recently large photovoltage of 0.7 V is reported in the multiferroic PFV bulk ceramics [130]. A strong visible-light PV effect is reported recently in a PFV ceramic based structure, Sn doped In_2O_3 (ITO)/PFV/ITO. The open circuit photovoltage in this material is negative and it varies from -0.45 V to -0.70 V. The photoresponse of PFV is shown in Fig. 22.

Table 2 summarizes the PV properties of different multiferroic systems. The band gap energy values of various multiferroic systems for PV application are shown in Fig. 23(a). Most of the multiferroics show their ferroic properties below room temperature which limits their practical applications. But the multiferroics recently investigated for PV applications are having ferroelectric and ferromagnetic transition temperatures above room temperature. The ferroic transition temperatures for different multiferroic PV materials are given in Fig. 23(b).

Table 2. PV responses of different multiferroic systems [44, 129].

Material	Photovoltage (V)	Photocurrent density (mAcm^{-2})	Light Intensity (mWcm^{-2})	Efficiency (%)
Ag/KBiFe ₂ O ₅ /Ag	8.8	0.015	4	-
STO:Nb/BFCO/ITO	0.74	0.990	1.5	6.5
STO/SRO/BFCO (Single layer)/ITO	0.79	11.7	100	3.3
STO/SRO:Nb/BFCO (Multilayers)/ITO	0.84	20.6	100	8.1

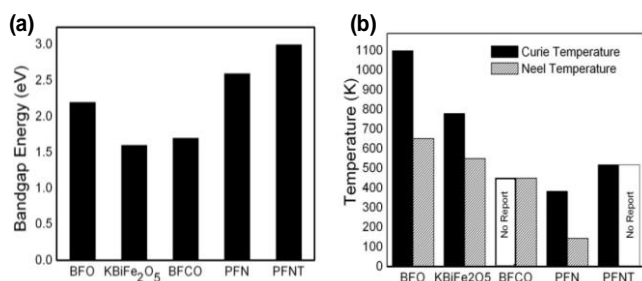


Fig. 23. (a) Bandgap energy values and (b) Curie and Neel temperatures for different multiferroic systems.

Preparation of ferroelectric and multiferroic photovoltaic materials

The physical properties of ferroelectric and multiferroics are highly dependent on the microstructure, defects and dislocations which are controlled by the preparation methods and processing parameters. For example, the absorption coefficient is controlled by defects such as oxygen vacancies which are controlled by heating conditions. So, the suitable selection of processing techniques and process parameters are very important to

tailor the properties of material for particular application. The optical parameters like refractive index, attenuation coefficient are highly dependent on the preparation method and substrate. It is discussed in the previous section how the optical, electrical and photovoltaic properties of the respective materials depend on the processing parameters. In the present section a brief description of the preparation methods commonly used to prepare the ferroelectric and multiferroic materials are reviewed here.

Preparation of PZT

Standard methods like solid state reaction [88] and sol gel [95] is mostly used to prepare PZT in its bulk form. For the preparation of PZT thin film RF sputtering [131], chemical solution deposition [132], laser ablation [133], metalorganic chemical vapor deposition (MOCVD) [93] have been extensively studied. The conventional solid state reaction method is a simplest method of PZT powder preparation. The high temperature processing sometimes result in low densification and improper stoichiometry due to lead loss (Pb/PbO) in PZT.

Sol-gel method addresses the issues associated with the preparation of PZT through solid state method. This method is widely used to prepare bulk PZT as well as thin film. Powder preparation through sol gel method is preferred because of good homogeneity and better stoichiometric control. In sol gel method the process temperature is comparatively low which enables the ease integration of PZT film with semiconducting materials that enhances photovoltaic properties. There may be some issues with pyrochlore phase formation in the thin film by sol gel method because of inter diffusion and oxygen content of the film. PZT prepared by hydrothermal method can suppress the inter diffusion and chemical reaction between film and substrate since it is a low temperature process (373 K- 473 K). This method is suitable for deposition of PZT on non planar surfaces [134-136].

Among the thin film preparation methods Pulsed Laser Deposition (PLD) is the best choice because of better stoichiometry. The nanostructured PZT thin films are generally prepared using PLD method to develop preferred photovoltaic structures [137]. Residual stresses are the main issue in thin film due to the structural and thermal misfit of the thin films and substrate. Optical properties in PZT are highly dependent on microstructure, crystal orientation, domain alignment and grain size. Optical properties strongly depend on the preparation method of PZT either in bulk or thin film form. A lowering (5%) of refractive index is observed in sol gel prepared PZT than the thin films prepared by MOCVD [138].

Preparation of BaTiO₃

The ferroelectric, optical and photovoltaic properties highly depend on microstructure, domain wall orientation, grain size and so on. So synthesis route has very much significance to determine its properties. Different methods like sol-gel, mechano-chemical, hydrothermal, Pechini, precipitation and oxalate co-precipitation including conventional solid state reaction method, were adopted to prepare bulk BT. Temperature and grain size dependent dielectric constant in ceramic BT is reported in many

papers [139]. The domain structure in BT also plays an important role to determine its properties. Mainly two types of domain walls are identified in tetragonal BT. 90° domain wall separates domains which are polarized perpendicularly to each other and 180° domain lies parallel to plane of the plate. Both types of domain walls are detected in BT [139].

The grain size has substantial influence on the dielectric permittivity. In BT ceramics (prepared via pressure less sintering and spark plasma sintering) dielectric constant increases with decrease in grain size (1–10 μm). Further decrease in grain size decreases the dielectric constant. The maximum value of dielectric constant (5000 or higher) is reported at a grain size of 2 μm which reveals a strong dependence of grain size on domain wall [140].

Use of dopants in BT decides the nature of conductivity, either p type or n type. Substitution of Ba^{2+} with monovalent, divalent and trivalent ions like Pb^{2+} , Sr^{2+} , Ca^{2+} and Cd^{2+} gives p type conductivity in BT. But substitution of Ti^{4+} with trivalent, tetravalent or pentavalent donor ions like Sn^{4+} , Hf^{4+} , Zr^{4+} , Ce^{4+} and Th^{4+} gives n type characteristics. Addition of donor dopants with valency higher than barium or titanium ions and at a relatively low donor ion concentration 0.15–0.3% (atomic percentage), leads to room-temperature semiconducting ceramics [141].

Preparation of LiNbO_3

LiNbO_3 is mainly grown in single crystal form by Czochralski technique from the congruent melt value of approximately 48.4 mol% Li_2O and an excess of Niobium as per stoichiometric of the compound [142]. Though it is widely used method for single crystal growth, but the method causes non stoichiometric defects in the crystal which degrades its quality. The stoichiometry in LiNbO_3 i.e., Li/Nb ratio is achieved through several post growth techniques, Vapor Transport Equilibration (VTE) technique is one the most used methods. Ceramic powders of LiNbO_3 can be prepared by solid state reaction method, ball milling and co precipitation method [143].

Chemical route of preparation is also reported for LiNbO_3 by dissolving the ingredient oxides to form complex structure which can dissolve in water. But dissolving niobium oxide is a big task as it takes a long time (~10 Hrs) [144]. Another method is combustion synthesis of LiNbO_3 powder [145]. The low temperature preparation of LiNbO_3 is possible through hydrothermal synthesis. Though the processing temperature of LiNbO_3 in hydrothermal synthesis is low (523 K), but it requires high dwelling time (24 Hrs). Molten salt method is reported as a simple method to prepare pure, stoichiometric LiNbO_3 powder at low temperature and in short time [146].

Preparation of KBNNNO

Bulk KBNNNO material is prepared by solid state reaction in powder form from its ingredient powders K_2CO_3 , BaCO_3 , NiO and Nb_2O_5 . Thin films of KBNNNO extracted from this pellets using focused ion beam and scanning electron microscope equipped with a lift out tool showed attractive photovoltaic properties mentioned in the above section [105].

Streaming Process for Electrode-less Electrochemical Deposition (SPEED) is used for KBNNNO thin film

preparation in a single step. This technique uses aqueous-based deposition process to deposit nanomaterials over large area surfaces. The advantage of this method is controlled growth rate (1 μmmin^{-1}), low temperature processing and air atmosphere [147]. Latest report shows that KBNNNO thin film developed on stainless steel by SPEED has excellent adhesion with the substrate after annealing at 923 K. This method could produce good quality microstructure compared to conventional solid state reaction method. An enhancement in electric polarization is reported in these films than the bulk KBNNNO . Higher polarization values and superior microstructure can improve the photoresponse in this FE material.

Preparation of BFO

Multiferroic BFO has been synthesized by different methods using oxide precursors and wet chemical methods. The different routes for the preparation of BFO using oxide precursors include conventional Solid state reaction [148–151] Rapid liquid sintering [152], and Mechanical activation [153] Solid state reaction method is most conventionally used for synthesizing oxide. But still it lacks uniformity of particle size, shape, and stoichiometry and produces many unwanted phases [154]. Rapid liquid sintering method finds advantage of formation of high resistive single phase BFO with saturated FE loops at room temperature [152]. The slow heating rate and long sintering time in conventional solid state reaction method of BFO result in the valence fluctuation of Fe ions from 3^+ to 2^+ along with oxygen vacancies leading to high leakage current which is in favor of PV application. It is well known that the leakage current in BFO is arising from the reduction of Fe^{3+} species to Fe^{2+} , creating oxygen vacancies for charge compensation [155]. But rapid liquid sintering method suppresses the formation of Fe^{2+} and oxygen deficiency and hence there is less leakage current. Mechanical activation of BFO significantly improves reactivity of the starting materials and enables the synthesis of BFO phase at relatively lower temperatures about 373 K lower than conventional solid-state-reaction method [152]. BFO has also been prepared by wet chemical methods like low temperature Sol-gel [154–156] Sonochemical, Hydrothermal, Microwave- Hydrothermal, Glycol gel reaction, Co-Precipitation, Modified Pechini, Polymer complex solution and Metal complexing methods to prepare different forms of BFO as single crystals, ceramics or thin films [154]. Out of these methods, sol-gel method is very useful for the preparation of phase pure BFO at low temperature as low as 673 K by using PVA [155, 156].

BFO thin films with most attractive multiferroic properties are mainly prepared by sputtering, radio frequency magnetron sputtering, Pulsed Laser Deposition (PLD) and Metal Organic Chemical Vapor Deposition (MOCVD) [157]. It is reported that the BFO thin films show very large values of remnant polarization when synthesized by PLD. BFO thin films grown epitaxially on SrTiO_3 (001) substrate showed a higher remnant polarization of about 60 μCcm^{-2} . A gigantic value for remnant polarization $P_r = 150 \mu\text{Ccm}^{-2}$ is observed with poly crystalline films grown on $\text{Pt/TiO}_2/\text{SiO}_2/\text{Si}$ substrates by PLD [158, 159]. The important advantage of using PLD or sputtering methods for the synthesis of BFO films is the

control of growth direction and texture of the films with respect to single crystal substrates and stoichiometry with good density and uniformity [160].

Preparation of BFCO

PLD is one of the most suitable techniques to grow complex oxides such as BFCO. BFCO is a metastable compound. PLD method allows the fabrication of non-equilibrium phases present in BFCO and the modification of their properties by strain engineering [109, 128]. The thin films of BFCO studied for photovoltaic properties are mainly prepared by PLD. The high volatility of Bi makes the deposition of BFCO through PLD very challenging. The growth of pure BFCO thin films on STO substrates is possible only in a narrow window of deposition parameters with fine controls of process parameters. The application of compressive epitaxial strain at sufficiently high temperatures allows the Fe and Cr cation arrangement in BFCO and thus promotes the long range cationic ordering. Of course, this cationic ordering involves a reduction of the cationic repulsion, shortens the chemical bonds, and reduces the unit cell volume which changes many functional properties.

Preparation of KBiFe_2O_5

KBiFe_2O_5 single crystals are prepared using $\text{Bi}(\text{NO}_3)_3$ and $\text{Fe}(\text{NO}_3)_3$ and KOH solutions and crystallized in an autoclave at 493 K [44].

Preparation of PFV

Bulk PFV is preferably prepared with conventional solid state reaction method. For the studies of photovoltaic property in this compound ITO has resulted out as the best electrode material [130].

Summary and future prospects

Ferroelectric and multiferroic photovoltaics is a very new and promising field of research. It has to mature and grow in leaps and bounds. Though efficiency of this class has to be improved to compete the present solar cell market, still, the application potential of these materials are tremendous because of their mutually dependent multiple functionalities. The merits of ferroelectric and multiferroic photovoltaic systems are multifold compared to the conventional photovoltaics. The scope of the present investigation is to explore an alternative energy source where efficiency of solar cell is not only a band gap dependent phenomenon and thus, overcome the theoretical efficiency of Shockley-Queisser limit. Recent developments in the field of oxide ferroelectric and multiferroics address the technical and economic issues of commercial solar cells. The essential need of building up p-n junction is no further a requirement of next generation solar cell and thus the efficiency of this kind of photovoltaics barely depends on bandgap. The possibility of coupling between PV and ferroelectricity/ferromagnetism or multicoupling between all functionalities makes this class fascinating for future research beyond its efficiency and capacity.

Reference

- Goetzberger, A.; Hebling, C. *Sol. Energ. Mat. Sol. C.* **2000**, *62*, 1.

- DOI: [10.1016/S0927-0248\(99\)00131-2](https://doi.org/10.1016/S0927-0248(99)00131-2)
- Yuan, Y.; Xiao, Z.; Yang, B.; Huang, J. *J. Mater. Chem. A.* **2014**, *2*, 6027.
DOI: [10.1039/c3ta14188h](https://doi.org/10.1039/c3ta14188h)
- Lewis, N.S. *Science* **2007**, *315*, 798.
DOI: [10.1126/science.1137014](https://doi.org/10.1126/science.1137014)
- Trupke, T.; Shalava, A.; Richardsa, B.S.; Wurfelb, P.; Green, M.A. *Sol. Energ. Mat. Sol. C.* **2006**, *90*, 3327.
DOI: [10.1016/j.solmat.2005.09.021](https://doi.org/10.1016/j.solmat.2005.09.021)
- Brown, G.F.; Wu, J. *Laser Photonics Rev.* **2009**, *3*, 394.
DOI: [10.1002/lpor.200810039](https://doi.org/10.1002/lpor.200810039)
- Green, M.A.; J. *Mater. Sci. Mater. Electron.* **2007**, *18*, 15.
DOI: [10.1007/s10854-007-9177-9](https://doi.org/10.1007/s10854-007-9177-9)
- Shah, A.; Torres, P.; Tscharnner, R.; Wyrsh, N.; Keppner, H. *Science* **1999**, *285*, 692.
DOI: [10.1126/science.285.5428.692](https://doi.org/10.1126/science.285.5428.692)
- Afzaal, M.; Brien, P.O. *J. Mater. Chem.* **2006**, *16*, 1597.
DOI: [10.1039/B512182E](https://doi.org/10.1039/B512182E)
- Jackson, P.; Hariskos, D.; Wuerz, R.; Kiowski, O.; Bauer, A.; Friedlmeier, T.M.; Powalla, M. *Phys. Status Solidi RRL* **2015**, *9*, 28.
DOI: [10.1002/pssr.201409520](https://doi.org/10.1002/pssr.201409520)
- Mathew, X.; Enriquez, J.P.; Romeo, A.; Tiwari, A.N. *Sol. Energ.* **2004**, *77*, 831.
DOI: [10.1016/j.solener.2004.06.020](https://doi.org/10.1016/j.solener.2004.06.020)
- Kumar, S.G.; Rao, K.S.R.K. *Energy Environ. Sci.* **2014**, *7*, 45.
DOI: [10.1039/C3EE41981A](https://doi.org/10.1039/C3EE41981A)
- Yoshimi, M.; Sasaki, T.; Sawada, T.; Suezaki, T.; Meguro, T.; Matsuda, T.; Santo, K.; Wadano, K.; Ichikawa, M.; Nakajima, A.; Yamamoto, K. 3rd World Conference on Photovoltaic Energy Conversion May 11-18, **2003** Osaka, Japan.
DOI: [10.1021/jz401532q](https://doi.org/10.1021/jz401532q)
- Hamakawa, Y.; Thin-Film Solar Cells: Next Generation Photovoltaics and Its Applications; Hamakawa, Yoshihiro (Ed.); Springer: Berlin, **2004**, pp-232.
- Gratzel, M. J. *Photoch. Photobio. C.* **2003**, *4*, 145.
DOI: [10.1155/2007/36970](https://doi.org/10.1155/2007/36970)
- Green, M.A.; Emery, K.; Hishikawa, Y.; Warta, W.; Dunlop, E. *Prog. Photovolt. Res. Appl.* **2013**, *21*, 827.
DOI: [10.1002/ppp.2404](https://doi.org/10.1002/ppp.2404)
- Wei, D. *Int. J. Mol. Sci.* **2010**, *11*, 1103.
DOI: [10.3390/ijms11031103](https://doi.org/10.3390/ijms11031103)
- Mathew, A.; Mohan, R.G.; Nookala, M. *Adv. Mat. Lett.* **2014**, *5*, 180.
DOI: [10.5185/amlett.2013.8527](https://doi.org/10.5185/amlett.2013.8527)
- Brabec, C.J.; Durrant, J.R. *Mrs. Bull.* **2008**, *33*, 670.
DOI: [10.1557/mrs2008.138](https://doi.org/10.1557/mrs2008.138)
- Chamberlain, G.A. *Solar Cells* **1983**, *8*, 47.
DOI: [10.1016/0379-6787\(83\)90039-X](https://doi.org/10.1016/0379-6787(83)90039-X)
- Pode, R. *Adv. Mat. Lett.* **2012**, *2*, 3.
DOI: [10.5185/amlett.2010.12186](https://doi.org/10.5185/amlett.2010.12186)
- Kamat, P.V. *J. Phys. Chem. C* **2008**, *112*, 18737.
DOI: [10.1021/jp806791s](https://doi.org/10.1021/jp806791s)
- Choubey, P.C.; Oudhia, A.; Dewangan, R. *Recent Research in Science and Technology* **2012**, *4*, 499.
- Rhile, S.; Shalom, M.; Zaban, A. *Chem. Phys. Chem* **2010**, *11*, 2290.
DOI: [10.1002/cphc.201000069](https://doi.org/10.1002/cphc.201000069)
- Park, N.G. *Materials Today* **2015**, *18*, 65.
DOI: [10.1016/j.mattod.2014.07.007](https://doi.org/10.1016/j.mattod.2014.07.007)
- Hoppea, H.; Sariciftci, N.S. *J. Mater. Res.*, **2004**, *19*, 1924.
DOI: [10.1557/JMR.2004.0252](https://doi.org/10.1557/JMR.2004.0252)
- Spanggaard, G.; Krebs, K.C. *Sol. Energ. Mat. Sol. Cells* **2004**, *83*, 125.
DOI: [10.1016/j.solmat.2004.02.021](https://doi.org/10.1016/j.solmat.2004.02.021)
- Kramer, I.J.; Minor, J.C.; Moreno-Bautista, G.; Rollny, L.; Kanjanaboos, P.; Kopilovic, D.; Thon, S.M.; Carey, G. H.; Chou, K. W.; Zhitomirsky, D.; Amassian, A.; Sargent, E. H. *Adv. Mater.* **2015**, *27*, 116.
DOI: [10.1002/adma.201403281](https://doi.org/10.1002/adma.201403281)
- Yang, S.Y.; Seidel, J.; Byrnes, S.J.; Shafer, P.; Yang, C.H.; Rossell, M.D.; Yu, P.; Chu, Y.H.; Scott, J.F.; Ager, Martin, L.W.; Ramesh, R. *Nat. Nanotechnol.* **2010**, *5*, 143.
DOI: [10.1038/nnano.2009.451](https://doi.org/10.1038/nnano.2009.451)
- Fridkin, V.M.; Popov, B. *Sov. Phys. Usp.* **1978**, *21*, 981.
DOI: [10.1070/PU1978v021n12ABEH005722](https://doi.org/10.1070/PU1978v021n12ABEH005722)

30. Ichiki, M.; Maeda, R.; Morikawa, Y.; Mabune, Y.; Nakada, T.; Nonaka, K. *Appl. Phys. Lett.* **2004**, *84*, 395.
DOI: [10.1143/JJAP.44.6927](https://doi.org/10.1143/JJAP.44.6927)
31. Bhatnagar, A.; Chaudhuri, A.R.; Kim, Y.H.; Hesse, D.; Alexe, M. *Nat. Commun.* **2013**, *4*, 2835.
DOI: [10.1038/ncomms3835](https://doi.org/10.1038/ncomms3835)
32. Yang, S.Y.; Martin, W.; Byrnes, S.J.; Conry, T.E.; Basu, S.R.; Paran, D.; Reichertz, Ihlefeld, J.; Adamo, C.; Melville, A.; Chu, Y.H.; Yang, C.-H.; Musfeldt, J. L.; Schlom, D. G.; Ager III, J. W.; Ramesh, R. *Appl. Phys. Lett.* **2009**, *95*, 062909.
DOI: [10.1063/1.3204695](https://doi.org/10.1063/1.3204695)
33. Alexe, M.; Hesse, D. *Nat. Commun.* **2011**, *2*, 256.
DOI: [10.1038/ncomms1261](https://doi.org/10.1038/ncomms1261)
34. Kreisel, J.; Alexe, M.; Thomas, P.A. *Nat. Mater.* **2012**, *11*, 260.
DOI: [10.1038/nmat3282](https://doi.org/10.1038/nmat3282)
35. Khomskii, D. *Trend: Physics* **2009**, *2*, 20.
DOI: [10.1103/Physics.2.20](https://doi.org/10.1103/Physics.2.20)
36. Ramesh, R.; Spaldin, N.A. *Nat. Mater.* **2007**, *6*, 21.
DOI: [10.1038/nmat1805](https://doi.org/10.1038/nmat1805)
37. Spaldin, N.A.; Cheong, S.-W.; Ramesh, R. *Phys. Today* **2010**, *63*, 38.
DOI: [10.1063/1.3502547](https://doi.org/10.1063/1.3502547)
38. Martin, L.W.; Crane, S.P.; Chu, Y.-H.; Holcomb, M.B.; Gajek, M.; Huijben, M.; Yang, C.-H.; Balke, N.; Ramesh, R. *Phys.: Condens. Matter* **2008**, *20*, 434220.
DOI: [10.1088/0953-8984/20/43/434220](https://doi.org/10.1088/0953-8984/20/43/434220)
39. Spaldin, N.A.; Fiebig, M.; *Science* **2005**, *309*, 391.
DOI: [10.1126/science.1113357](https://doi.org/10.1126/science.1113357)
40. Scott, J.F. *Nat. Mater.* **2007**, *6*, 256.
DOI: [10.1038/nmat1868](https://doi.org/10.1038/nmat1868)
41. Manuel, B.; Agnès, B. *Nat. Mater.* **2008**, *7*, 425.
DOI: [10.1038/nmat2189](https://doi.org/10.1038/nmat2189)
42. Gajek, M.; Bibes, M.; Fusil, S.; Bouzouane, K.; Fontcuberta, J.; Agnès, B.; Fert, A.; *Nat. Mater.* **2007**, *6*, 96.
DOI: [10.1038/nmat1860](https://doi.org/10.1038/nmat1860)
43. Béa, H.; Gajek, M.; Bibes, M.; Barthélémy, A. *J. Phys.: Condens. Matter* **2008**, *20*, 434221.
DOI: [10.1088/0953-8984/20/43/434221](https://doi.org/10.1088/0953-8984/20/43/434221)
44. Zhang, G.; Wu, H.; Li, G.; Huang, Q.; Yang, C.; Liao, F.H.F.; Lin, J. *Sci. Rep.* **2013**, *3*, 1265.
DOI: [10.1038/srep01265](https://doi.org/10.1038/srep01265)
45. Roy, A.; Gupta, R.; Garg, A. *Adv. Cond. Matter. Phys.* **2012**, *2012*, 926290.
DOI: [10.1155/2012/926290](https://doi.org/10.1155/2012/926290)
46. Tokura, Y. *J. Magn. Magn. Mater.* **2007**, *310*, 1145.
DOI: [10.1016/j.jmmm.2006.11.198](https://doi.org/10.1016/j.jmmm.2006.11.198)
47. Khomskii, D.I. *J. Magn. Magn. Mater.* **2006**, *306*, 1.
DOI: [10.1016/j.jmmm.2006.01.238](https://doi.org/10.1016/j.jmmm.2006.01.238)
48. Brody, P.S.; Crowne, F. *J. Electron. Mater.* **1975**, *4*, 955.
DOI: [10.1007/BF02660182](https://doi.org/10.1007/BF02660182)
49. Ichiki, M.; Furue, H.; Kobayashi, T.; Maeda, R. *Appl. Phys. Lett.* **2005**, *87*, 222903.
DOI: [10.1063/1.2128479](https://doi.org/10.1063/1.2128479)
50. Butler, K.T.; Frost, J.M.; Walsh, A.; *Energy Environ. Sci.* **2015**, *8*, 838.
DOI: [10.1039/c4ee03523b](https://doi.org/10.1039/c4ee03523b)
51. Belinicher, V.I.; Sturman, B.I. *Sov. Phys. Usp* **1980**, *23*, 199.
DOI: [10.1070/PU1980v023n03ABEH004703](https://doi.org/10.1070/PU1980v023n03ABEH004703)
52. Lines, M. E.; Glass, A. M. *Principles and Applications of Ferroelectrics and Related Materials*, Clarendon Press, Oxford, 1977.
53. Fridkin, V.M. *Crystallogr. Rep.* **2001**, *46*, 654.
DOI: [10.1134/1.1387133](https://doi.org/10.1134/1.1387133)
54. Fridkin, V.M. *Appl. Phys.* **1977**, *13*, 357.
DOI: [10.1007/BF00882610](https://doi.org/10.1007/BF00882610)
55. Chynoweth, A.G. *Phys. Rev.* **1956**, *102*, 705.
DOI: [10.1103/PhysRev.102.705](https://doi.org/10.1103/PhysRev.102.705)
56. Huang, H. *Nat. Photonics* **2010**, *4*, 134.
DOI: [10.1038/nphoton.2010.15](https://doi.org/10.1038/nphoton.2010.15)
57. Young, S.M.; Rappe, A.M. *Phys. Rev. Lett.* **2012**, *109*, 116601.
DOI: [10.1103/PhysRevLett.109.116601](https://doi.org/10.1103/PhysRevLett.109.116601)
58. Seidel, J.; Fu, D.; Yang, S.-Y.; Llado, E.A.; Wu, J.; Ramesh, R.; Ager, J.W. *Phys. Rev. Lett.* **2011**, *107*, 126805.
DOI: [10.1103/PhysRevLett.107.126805](https://doi.org/10.1103/PhysRevLett.107.126805)
59. Poosanaas, P.; Tonooka, K.; Uchino, K.; *Mechatronics*, **2000**, *10*, 467.
60. Sung, J.H.; Lee, W.-M.; Lee, J.H.; Chu, K.; Lee, D.; Moya, X.; Mathur, N.D.; Yang, C.-H.; Park, J.-H.; Jo, M.-H. *NPG Asia Mater.* **2013**, *5*, e38.
DOI: [10.1038/am.2013.1](https://doi.org/10.1038/am.2013.1)
61. Cao, D.; Xu, J.; Fang, L.; Dong, W.; Zheng, F.; Shen, M. *Appl. Phys. Lett.* **2010**, *96*, 192101.
DOI: [10.1063/1.3427500](https://doi.org/10.1063/1.3427500)
62. Schafrank, R.; Payan, S.; Maglione, M.; Klein, A. *Phys. Rev. B* **2008**, *77*, 195310.
DOI: [10.1103/PhysRevB.77.195310](https://doi.org/10.1103/PhysRevB.77.195310)
63. Chen, B.; Zuo, Z.; Liu, Y.; Zhan, Q.-F.; Xie, Y.; Yang, H.; Dai, G.; Li, Z.; Xu, G.; Li, R.-W. *Appl. Phys. Lett.* **2012**, *100*, 173903.
DOI: [10.1063/1.4709406](https://doi.org/10.1063/1.4709406)
64. Ichiki, M.; Maeda, R.; Morikawa, Y.; Mabune, Y.; Nakada, T.; Nonaka, K.; *Appl. Phys. Lett.* **2004**, *84*, 395.
DOI: [10.1080/00150193.2011.620888](https://doi.org/10.1080/00150193.2011.620888)
65. Yao, K.; Gan, B. K.; Chen, M.; Shannigrahi, S.; *Appl. Phys. Lett.* **2005**, *87*, 212906.
DOI: [10.1063/1.2136228](https://doi.org/10.1063/1.2136228)
66. Nechache, R.; Harnagea, C.; Licoccia, S.; Traversa, E.; Ruediger, A.; Pignolet, A.; Rosei, F. *Appl. Phys. Lett.* **2011**, *98*, 202902.
DOI: [10.1063/1.3590270](https://doi.org/10.1063/1.3590270)
67. Zheng, F.G.; Xu, J.; Fang, L.; Shen, M.R.; Wu, X.L. *Appl. Phys. Lett.* **2008**, *93*, 172101.
DOI: [10.1063/1.3009563](https://doi.org/10.1063/1.3009563)
68. Qin, M.; Yao, K.; Liang, Y.C. *Appl. Phys. Lett.* **2008**, *93*, 122904.
DOI: [10.1063/1.2990754](https://doi.org/10.1063/1.2990754)
69. Dong, W.; Guon, Y.; Guo, B.; Liu, H.; Li, H. *Mater. Lett.* **2013**, *91*, 359.
DOI: [10.1016/j.matlet.2012.10.031](https://doi.org/10.1016/j.matlet.2012.10.031)
70. Chen, B.; Li, M.; Liu, Y.; Zuo, Z.; Zhuge, F.; Zhan, Q.-F.; Li, R.-W. *Nanotechnology* **2011**, *22*, 195201.
DOI: [10.1088/0957-4484/22/19/195201](https://doi.org/10.1088/0957-4484/22/19/195201)
71. Yarmarkin, V.; Gol'tsman, B.; Kazanin, M.; Lemanov, V. *Phys. Solid State* **2000**, *42*, 522.
DOI: [10.1134/1.1131242](https://doi.org/10.1134/1.1131242)
72. Choi, T.; S. Lee.; Choi, Y.J.; Kiryukhin, V.; Cheong, S.W. *Science* **2009**, *324*, 63.
DOI: [10.1126/science.1168636](https://doi.org/10.1126/science.1168636)
73. Ji, W.; Yao, K.; Liang, Y. C. *Adv. Mater.* **2010**, *22*, 1763.
DOI: [10.1002/adma.200902985](https://doi.org/10.1002/adma.200902985)
74. Qu, T.L.; Zhao, Y.G.; Xie, D.; Shi, J.P.; Chen, Q.P.; Ren, T.L. *Appl. Phys. Lett.* **2011**, *98*, 173507.
DOI: [10.1063/1.3584031](https://doi.org/10.1063/1.3584031)
75. Cao, D.; Wang, C.; Zheng, F.; Dong, W.; Fang, L.; Shen, M. *Nano Lett.* **2012**, *12*, 2803.
DOI: [10.1021/nl300009z](https://doi.org/10.1021/nl300009z)
76. Even, J.; Pedesseau, L.; Jancu, J.-M.; Katan, C. *J. Phys. Chem. Lett.* **2013**, *4*, 2999.
DOI: [10.1021/jz401532q](https://doi.org/10.1021/jz401532q)
77. Olsson, P.; Domain, C.; Guillemoles, J.-F. *Phys. Rev. Lett.* **2009**, *102*, 227204.
DOI: [10.1103/PhysRevLett.102.227204](https://doi.org/10.1103/PhysRevLett.102.227204)
78. Ganichev, S.D.; Ivchenko, E.L.; Bel'kov, V.V.; Tarasenko, S.A.; Sollinger, M.; Weiss, D. *Nature* **2002**, *417*, 153.
DOI: [10.1038/417153a](https://doi.org/10.1038/417153a)
79. Fedorov, A.; Pershin, Y.V.; Piermarocchi, C. *Phys. Rev. B* **2005**, *72*, 245327.
DOI: [10.1103/PhysRevB.72.245327](https://doi.org/10.1103/PhysRevB.72.245327)
80. Ziese, M.; Thornton, M.J. *Spin Electronics (Lecture Notes in Physics)*; Springer: Verlag, **2001**.
81. Young, M.N.; Zheng, F.; Rappe, A.M. *Phys. Rev. Lett.* **2013**, *110*, 057201.
DOI: [10.1103/PhysRevLett.110.057201](https://doi.org/10.1103/PhysRevLett.110.057201)
82. Koch, W.T.H.; Munser, R.; Ruppel, W.; Würfel, P. *Solid State Commun.* **1975**, *17*, 847.
DOI: [10.1016/0038-1098\(75\)90735-8](https://doi.org/10.1016/0038-1098(75)90735-8)
83. Zenkevich, A.; Matveyev, Y.; Maksimova, K.; Gaynutdinov, R.; Tolstikhina, A.; Fridkin, V.; *Phys. Rev. B* **2014**, *90*, 161409.
84. Wemple, S. H.; Didomenico, M.; Camlibel, I. *J. Phys. Chem. Solids* **1968**, *29*, 1797.
85. Zheng, F.; Xin, Y.; Huang, W.; Zhang, J.; Wang, X.; Shen, M.; Dong, W.; Fang, L.; Bai, Y.; Shen, X.; Hao, J. *J. Mater. Chem. A.* **2014**, *2*, 1363.
86. Zhang, J.; Su, X.; Zou, G. *Sci. Rep.* **2013**, *3*, 2109.
DOI: [10.1038/srep02109](https://doi.org/10.1038/srep02109)

87. Phungsiheng, S.; Sanorpim, S.; Wasanapiarnpong, T. *J. Sci. Technol.* **2013**, *20*, 109.
88. Boukamp, B.A.; Pham, M.T.N.; Blank, D.H.A.; Bouwmeester, H.J.M.; *Solid State Ion.* **2004**, *174*, 239.
DOI: [10.1016/j.ssi.2004.03.005](https://doi.org/10.1016/j.ssi.2004.03.005)
89. Moret, M.P.; Devillers, K.; Devillers, M.A.C.; Wo'rthoff, K.; Larsen, P.K. *J. Appl. Phys.* **2002**, *92*, 468.
DOI: [10.1063/1.1486048](https://doi.org/10.1063/1.1486048)
90. Qin, M.; Yao, K.; Liang, Y.C. *Appl. Phys. Lett.* **2008**, *93*, 122904.
DOI: [10.1063/1.2990754](https://doi.org/10.1063/1.2990754)
91. Camargo, A. S. S. de; Botero, E. R. ; Garcia, D.; Eiras, J. A.; Nunes, L.A.O. *Appl. Phys. Lett.* **2005**, *86*, 152905.
92. Scott, J.C.; *Ferroelectric Memories*; Springer: England, **2000**.
93. Peng, C.H.; Optical property studies and metalorganic chemical vapor deposition of Ferroelectric lead zirconate titanate thin films, Doctoral Dissertations, **1992**.
94. Shih, J.-L.; Cheung, M.C.-K.; Kruger, S.E.; Jen, C.-K. Electrical and optical properties of pzt thick films in high temperature flexible ultrasonic transducers for structural health monitoring and NDT International Workshop, CANSIMART CINDE IZFP, Canada, **2011**.
95. Aulika, I; Zauls, Kundzins, V.K; Kundzins, K; Katholy, S. J. *Optoelectron. Adv. M.* **2003**, *5*, 755-761.
96. Zheng, F.; Zhang, P; Wang, X; Huang, W.; Zhang, J.; Shen, d-M.; Dong, W.; Fang, L.; Bai, Xiaoqing Shen, Y.; Sun, H.; Hao, J.; *Nanoscale*, **2014**, *6*, 2915.
DOI: [10.1039/C3NR05757G](https://doi.org/10.1039/C3NR05757G)
97. Chvostov, D.; Pajasova; L.; Zelezny, V. *Phys. stat. sol.* **2008**, *5*, 1362.
DOI: [10.1002/pssc.200777869](https://doi.org/10.1002/pssc.200777869)
98. Pandey, S.K.; James, A.R; Raman, R.; Chatterjee, S.N.; Goyal, A.; Prakash, C.; Goel, T.C. *Physica B* **2005**, *369*, 135.
99. Koch, W.T.H.; Munser, R.; Ruppel, W.; Würfel, P. *Solid State Commun.* **1975**, *17*, 847.
DOI: [10.1016/0038-1098\(75\)90735-8](https://doi.org/10.1016/0038-1098(75)90735-8)
100. Kim, S.R.; Choi, S.K.; Lee, H.M. *J. Mater. Res.* **2000**, *15*, 1354.
DOI: [10.1557/JMR.2000.0197](https://doi.org/10.1557/JMR.2000.0197)
101. Zenkevich, A.; Matveyev, Y.; Maksimova, K.; Gaynutdinov, R.; Tolstikhina, A.; Fridkin, V.; *Phys. Rev. B* **2014**, *90*, 161409.
102. Cai, W.; Fu, C.; Gao, J.; Guo, Q.; Deng, X.; Zhang, C.; *Physica: B* **2011**, *406*, 3583.
DOI: [10.1016/j.physb.2011.06.041](https://doi.org/10.1016/j.physb.2011.06.041)
103. Dharmadhikari, V.S.; Grannemann, W.W. *J. Appl. Phys.* **1982**, *53*, 8988.
DOI: [10.1063/1.330456](https://doi.org/10.1063/1.330456)
104. Lu, Z.; Zhao, K.; Li, X. *Ferroelectrics-Physical Effects*; Lallart, M. (Eds.); InTech: **2011**, 1-666.
DOI: [10.5772/942](https://doi.org/10.5772/942)
105. Grinberg, I.; West, D.V.; Torres, M.; Gou, G.; Stein, D.M.; Liyan Wu, Chen, G.; Gallo, E.M.; Akbashev, E.R.; Davies, P.K.; Spanier, J.E.; Rappe, A.M. *Nature*, **2013**, *503*, 509.
DOI: [10.1038/nature12622](https://doi.org/10.1038/nature12622)
106. Wang Y.; Jiang, Q.-h.; He, H.-c.; Nan, C.W. *Appl. Phys. Lett.* **2006**, *88*, 142503.
DOI: [10.1063/1.2191947](https://doi.org/10.1063/1.2191947)
107. Kornev, I.A.; Bellaiche, L. *Phys. Rev. B* **2009**, *79*, 100105(R).
DOI: [10.1103/PhysRevB.79.100105](https://doi.org/10.1103/PhysRevB.79.100105)
108. Wang, D.H.; Yan, L.; Ong, C.K.; Du, Y.W. *Appl. Phys. Lett.* **2006**, *89*, 182905.
DOI: [10.1063/1.2374805](https://doi.org/10.1063/1.2374805)
109. Martin, L.W.; Chu, Y.-H.; Zhan, Q.; Ramesh, R.; Han, S.-J.; Wang, S.X.; Warusawithana, M.; Schlom, D.G. *Appl. Phys. Lett.* **2007**, *91*, 172513.
DOI: [10.1063/1.2801695](https://doi.org/10.1063/1.2801695)
110. Vengalis, B.; Sliuziene, K. *Mater.Sci.* **2011**, *17*, 1392.
DOI: [10.5755/j01.ms.17.4.769](https://doi.org/10.5755/j01.ms.17.4.769)
111. Shima, H.; Naganuma, H.; Okamura, S. *Materials Science - Advanced Topics*, Prof. Yitzhak Mastai (Ed.), InTech, **2013**, 33.
DOI: [10.5772/5490](https://doi.org/10.5772/5490)
112. Jin, K.X.; Li, Y.F.; Wang, Z.L.; Peng, H.Y.; Lin, W.N.; Kyaw, A.K.K.; Jin, Y.L.; Jin, K.J.; Sun, X.W.; Soci, C.; Wu, T. *AIP Adv.* **2012**, *2*, 042131.
DOI: [10.1063/1.4766279](https://doi.org/10.1063/1.4766279)
113. Chu, Y.-H.; Cruz, M.P.; Yang, C.-H.; Martin, L. W.; Yang, P.-L.; Zhang, J.-X.; Lee, K.; Yu, P.; Chen, L.-Q.; Ramesh, R. *Adv. Mater.* **2007**, *19*, 2662.
DOI: [10.1002/adma.200602972](https://doi.org/10.1002/adma.200602972)
114. Setter, N.; Damjanovic, D.; Eng, L.; Fox, G.; Gevorgian, S.; Hong, S.; Kingon, A.; Kohlstedt, H.; Park, N.Y.; Stephenson, G.B.; Stolitchnov, I.; TagansteV, A.K.; Taylor, D.V.; Yamada, T.; Streiffer, S. *J. Appl. Phys.* **2006**, *100*, 051606.
DOI: [10.1063/1.2336999](https://doi.org/10.1063/1.2336999)
115. Sheu, Y.M.; Trugman, S.A. ; Park, Y.-S. ; Lee, S.; Yi, H.T. ; Cheong, S.-W. ; Jia, Q.X.; Taylor, A.J.; Prasankumar, R.P. *Appl. Phys. Lett.* **2012**, *100* 242904.
DOI: [10.1063/1.4729423](https://doi.org/10.1063/1.4729423)
116. Prashanthi, K.; Dhandharia, P.; Miriyala, N.; Gaikwad. R.; Barlage, D.; Thundat, T. *Nano Energy* **2015**, *13*, 240.
DOI: [10.1016/j.nanoen.2015.02.014](https://doi.org/10.1016/j.nanoen.2015.02.014)
117. Ukai, Y.; Yamazaki, S.; Kawae, T.; Morimoto, *Jpn. J. Appl. Phys.* **2012**, *51*, 09LE10.
DOI: [10.1143/JJAP.51.09LE10](https://doi.org/10.1143/JJAP.51.09LE10)
118. Khan, G.G.; Das, R.; Mukherjee, N.; Mandal, K. *Phys. Status Solidi RRL* **2012**, *6*, 312.
DOI: [10.1002/pssr.201206211](https://doi.org/10.1002/pssr.201206211)
119. Bharathi, K.K.; Lee, W.-M.; Sung, J.H.; Lim, J.S.; Kim, S.J.; Chu, K.; Park, J.W.; Song, J.H.; Jo, M.-H.; Yang, C.-H. *Appl. Phys. Lett.* **2013**, *102*, 012908.
DOI: [10.1063/1.4774381](https://doi.org/10.1063/1.4774381)
120. Lotey, G.S.; Verma, N.K. *Chem. Phys. Lett.* **2013**, *574*, 71.
DOI: [10.1016/j.cplett.2013.04.046](https://doi.org/10.1016/j.cplett.2013.04.046)
121. Xu, Z.-R.; Tu, C.S.; Hung, C.-M.; Ting, Y.; Chen, P.-Y. *IEEE T. Magn.* **2014**, *50*, 2500304.
DOI: [10.4236/mrc.2013.23A001](https://doi.org/10.4236/mrc.2013.23A001)
122. Katiyar, R. K. ; Sharma, Y.; Barrionuevo, D.; Kooriyattil, S.; Pavunny, S. P. ; Young, J. S. ; Morell, J. S. ; Weiner, B. R.; Katiyar, R.S.; Scott, J.F. *Appl. Phys. Lett.* **2015**, *106*, 082903.
DOI: [10.1063/1.4908254](https://doi.org/10.1063/1.4908254)
123. Chakrabarty, J.; Nechache, R.; Li, S.; Nicklaus, M.; Ruediger, A.; Rosei, F. *J. Am. Ceram. Soc.* **2014**, *97*, 1837.
DOI: [10.1111/jace.12837](https://doi.org/10.1111/jace.12837)
124. Gupta, S.; Tomar, V.; Gupta, M.; *J. Appl. Phys.* **2014**, *115*, 014102.
DOI: [10.1063/1.4859575](https://doi.org/10.1063/1.4859575)
125. Zang, Y.; Xie, D.; Wu, X.; Chen, Y.; Lin, Y.; Li, M.; Tian, H.; Li, X.; Li, Z.; Zhu H.; Ren, T.; Plant, D. *Appl. Phys. Lett.* **2011**, *99*, 132904.
DOI: [10.1063/1.3644134](https://doi.org/10.1063/1.3644134)
126. Kundys, B.; Viret, M.; Colson, D.; Kundys, D.O. *Nat. Mater.* **2010**, *9*, 803.
DOI: [10.1038/nmat2807](https://doi.org/10.1038/nmat2807)
127. Nechache, R.; Harnagea, C.; Carignan, L.P.; Gautreau, O.; Pintilie, L.; Singh, M.; Ménard, D.; Fournier, P.; Alexe, M.; Pignolet, A. *J. Appl. Phys.* **2009**, *105*, 061621.
DOI: [10.1063/1.3073826](https://doi.org/10.1063/1.3073826)
128. Nechache, R.; Harnagea, C.; Li, S.; Cardenas, L. Huang, W.; Chakrabarty, J. Rosei, F. *Nature Photon.* **2015**, *9*, 61.
DOI: [10.1038/nphoton.2014.255](https://doi.org/10.1038/nphoton.2014.255)
129. Nechache, R.; Rosei, F. *J. Solid State Chem.* **2012**, *189*, 13.
DOI: [10.1016/j.jssc.2012.01.022](https://doi.org/10.1016/j.jssc.2012.01.022)
130. Wu, Z.; Zhang, Y.; Ma, K.; Cao, Y.; Lin, H.; Jia, Y.; Chen, J.; Li, H. *Phys. Status Solidi RRL* **2014**, *8*, 36.
DOI: [10.1002/pssr.201308259](https://doi.org/10.1002/pssr.201308259)
131. Bruchhaus, R.; Huber, H.; Pitzer, D.; Wersing, W. *Ferroelectrics* **1992**, *127*, 137.
DOI: [10.1080/0015019920822336](https://doi.org/10.1080/0015019920822336)
132. Pontes, F.M.; Leite, M.S.J. Nunes, D.S.L.; Pontes, D.; Longo, E.; Magnani, P.S. Pizani, E.; Varela, J.A. *J. Eur. Ceram. Soc.* **2004**, *24*, 2969.
DOI: [10.1016/S0955-2219\(03\)00318-2](https://doi.org/10.1016/S0955-2219(03)00318-2)
133. Zhou, Y.C.; Yang, Z.Y.; Zheng, X.J.; Li, J.Y. Residual stress in piezoelectric thin film prepared by pulse laser beam ablation, *ICF10*, Honolulu (USA)2001, **2013**.
134. Cao, D.; Fang, J.X.L.; Dong, W.; Zhenga, F.; Shenb, M. *Appl. Phys. Lett.* **2010**, *96*, 192101.
DOI: [10.1063/1.3427500](https://doi.org/10.1063/1.3427500)
135. Y. Zang, D. Xie, Y. Chen, X. Wu, T. Ren, H. Zhu, J.-L. Cao, D. Plant, *J. Appl. Phys.* **2012**, *112*, 054103.
136. Wang, D.G.; Chen, C.Z.; Ma, J.; Liu, T.H. *Appl. Surf. Sci.* **2008**, *255*, 1637.
137. Lin, Y., Zhao, B. R., Peng, H. B., Hao, Z., Xu, B., Zhao, Z. X.; Chen, J. S., *J. Appl. Phys.* **1999**, *86*, 4467.
DOI: [10.1063/1.371388](https://doi.org/10.1063/1.371388)

138. Lappalainen, J.; Hiltunen, J.; Lantto, V. *J. Eur. Ceram. Soc.* **2005**, *25*, 2273.
DOI: [10.1016/j.jeurceramsoc.2005.03.044](https://doi.org/10.1016/j.jeurceramsoc.2005.03.044)
139. Vijatović, M. M.; Bobić, J. D.; Stojanović, B. D. *Sci. Sinter.* **2008**, *40*, 235.
DOI: [10.2298/SQS0803235V](https://doi.org/10.2298/SQS0803235V)
140. Ghosh, D.; Sakata, A.; Carter, J.; Thomas, P.A.; Han, H.; Nino, J.C.; Jones, J.L. *Adv. Funct. Mater.* **2014**, *24*, 885.
DOI: [10.1002/adfm.201301913](https://doi.org/10.1002/adfm.201301913)
141. Chen, Y.-C. *J. Mater. Sci. Technol.* **2007**, *15*, 307.
142. Chen, Y.; Zhang, W.; Shu, Y.; Lou, C.; Huang, Y.K.Z.; Xu, J.; Zhang, G. *Opt. Mater.* **2003**, *23*, 295.
DOI: [10.1016/S0925-3467\(02\)00305-1](https://doi.org/10.1016/S0925-3467(02)00305-1)
143. Prakash, B.J.; Buddhudu, S. *JJPAP* **2012**, *50*, 320.
144. Camargo, E.R.; Kakihana, M. *Solid State Ion.* **2002**, *151*, 413.
145. Liu, M.N.; Xue, D.F.; Zhang, S.C.; Zhu, H.Y. *Mater. Lett.* **2005**, *59*, 1095.
DOI: [10.1016/j.matlet.2004.12.015](https://doi.org/10.1016/j.matlet.2004.12.015)
146. Yu, J.; Liu, X.Q. *Chemical Journal of Chinese Universities* **2005**, *26*, 595.
DOI: [10.1021/jz302048d](https://doi.org/10.1021/jz302048d)
147. Rezaie, F.K.; Panjwani, D.; Natha, J.; Fredricksena, C.J.; Oladejib, I.O.; Pealea, R.E.; Proc. SPIE 9115, Energy Harvesting and Storage: Materials, Devices, and Applications V, 91150Q, **2014**.
DOI: [10.1117/12.2050707](https://doi.org/10.1117/12.2050707)
148. Bhole, C.P.; Patil, S.L.; Rewatkar, K.G; International Conference on Benchmarks in Engineering Science and Technology ICBEST 2012, IJCA, **2012**.
149. Bhole, C.P.; *Archives of Applied Science Research* **2011**, *3*, 384.
150. Bhole, C.P. *Ceramics- Silikáty* **2012**, *56*, 127.
151. Wang, Y.P.; Zhou, L.; Zhang, M.F.; Chen, X.Y; Liu, J-M.; Liua, Z.G. *Appl. Phys. Lett.* **2004**, *84*, 1731
DOI: [10.1063/1.1667612](https://doi.org/10.1063/1.1667612)
152. Maurya, D.; Thota, H.; Nalwa, K.S.; Garg, A. *J. Alloy. Comp.* **2009**, *477*, 780.
DOI: [10.1016/j.jallcom.2008.10.155](https://doi.org/10.1016/j.jallcom.2008.10.155)
153. Silva, J.; Reyes, A.; Esparza, H.; Camacho, H.; Fuentes, L. *Integr. Ferroelectr.* **2011**, *126*, 47.
DOI: [10.1080/10584587.2011.574986](https://doi.org/10.1080/10584587.2011.574986)
154. Suresh, P.; Srinath, S. *Adv. Mat. Lett.* **2014**, *5*, 127.
DOI: [10.5185/amlett.2013.fdm.34](https://doi.org/10.5185/amlett.2013.fdm.34)
155. Liu, H.; Liu, Z.; Yao, K.; *J. Sol-Gel Sci Techn* **2007**, *41*, 123.
DOI: [10.1007/s10971-006-0514-x](https://doi.org/10.1007/s10971-006-0514-x)
156. Liu, T. *J. Am. Ceram. Soc.* **2010**, *93*, 3637.
DOI: [10.1111/j.1551-2916.2010.03945.x](https://doi.org/10.1111/j.1551-2916.2010.03945.x)
157. Chaodan, Z.; Duanming, Z.; Jun, Y.; Bin, Y.; Yunyi, W.; Longhai, W.; Yunbo, W.; Wenli, Z. *Integr. Ferroelectr.* **2007**, *94*, 23.
DOI: [10.1080/10584580701755815](https://doi.org/10.1080/10584580701755815)
158. Park, J.M.; Gotoda, F.; Kanashima, T.; Okuyama, M.; Nakashima, S. *J. Korean Phys. Soc.* **2011**, *59*, 2537.
DOI: [10.3938/jkps.59.2537](https://doi.org/10.3938/jkps.59.2537)
159. Naganuma, Y.H.; Kovacs, A.; Hirata, A.; Hirotsu, Y.; Okamura, S. *Mater. Trans.* **2007**, *48*, 2370.
DOI: [10.1080/10584580701759411](https://doi.org/10.1080/10584580701759411)
160. Cha, J.O.; Ahn, J.S.; Leey, K.W.B.A. *J. Korean Phys. Soc.* **2009**, *54*, 844.

Advanced Materials Letters

Copyright © VBRI Press AB, Sweden

www.vbripress.com

Publish your article in this journal

Advanced Materials Letters is an official international journal of International Association of Advanced Materials (IAAM, www.iaamonline.org) published by VBRI Press AB, Sweden monthly. The journal is intended to provide top-quality peer-review articles in the fascinating field of materials science and technology particularly in the area of structure, synthesis and processing, characterisation, advanced-state properties, and application of materials. All published articles are indexed in various databases and are available download for free. The manuscript management system is completely electronic and has fast and fair peer-review process. The journal includes review article, research article, notes, letter to editor and short communications.

